Supporting information

Exploiting zinc(II) and copper(II) fluorescent complexes for enantiomeric excess determination of hydroxycarboxylates

Sara Sheykhi,[a] Lorenzo Mosca,[b] Mariia Pushina,[a] Kaustav Dey,[a] and Pavel Anzenbacher, Jr.[a,*]

[a] Department of Chemistry, Bowling Green State University Bowling Green, OH 43403, USA
[b] Department of Chemistry, Northwestern University, Evanston, IL 60208, USA

E-mail: pavel@bgsu.edu

Table of Contents

1. Chemicals and Instrumentation

All chemicals were analytical grade and they were used without purification. ^{1}H- and ^{13}C-NMR spectra were measured with a Bruker® Avance II™ 500MHz UltraShield™ (Bruker Corporation, Mass., USA) spectrometer operating at 11.7 T. The chemical shifts (δ) were referenced to the respective solvent and splitting patterns were designated as *s* (singlet), *d* (doublet), *t* (triplet), *m* (multiplet). Mass-spectrometry studies were performed using a Shimadzu MS-8030 equipped with an electron spray ionization (ESI) source and a triple quadrupole mass analyzer or a Shimadzu Axima Performance Matrix-assisted laser desorption ionization-time of flight (MALDI-TOF) mass spectrometer. Quantum yields were recorded by using a Hamamatsu Quantaurus QY-C11347 absolute quantum yield integrating sphere. The pH value of the solvent was measured with a Titrator T50 (Mettler Toledo Co.). All titrations and enantiomeric excess calibration curves were measured at 25°C in a 7:3 MeCN/H_2O solution, buffered to pH = 6 (50 mM MES). Fluorescence measurements were performed on a single photon counting spectrofluorimeter from Edinburgh Analytical Instruments (FL/FS 920). Solutions of the chiral sensors were excited at 444 nm. Fluorescence emission spectra were recorded between 455 nm and 600 nm. The band passes of excitation and emission monochromators were set to 1.0 nm. Wavelength sampling was 1 nm. Dwell time was set to 0.20 sec. All titrations were performed by dissolving the corresponding hydroxycarboxylic acid in a solution of the sensor in MeCN/H_2O (7:3, v/v, pH = 6); [Zn-complex] = 20 μM, [Cu-complex] = 780 μM, [C343] = 0.01 μM. Titration isotherms were constructed from changes in the fluorescence maximum at 492 nm. Data analysis and curve fitting was performed according to previously published methods.[1] All errors on binding constants were < 25 %.

Preparation of buffered solutions. 2-morpholin-4-ylethanesulfonic acid (MES; 2.44 g, 50 mmol) was dissolved in MeCN/H_2O (7/3, v/v, 200 mL). The pH of the solution was adjusted to 6 with NaOH (2 M). The solution was filtered and diluted to 250 mL with 7:3 MeCN/H_2O.

2. Synthesis

2.1 Synthesis of (1S,2S)- and (1R,2R)-N^1,N^2-bis(quinolin-2-ylmethylene)cyclohexane-1,2-diimine (1).

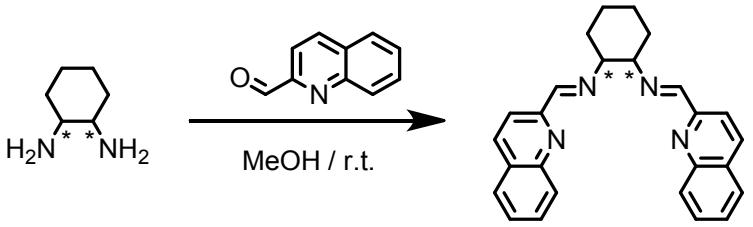

1*

Schiff base **1** was synthesized according to a modified literature procedure.[1] In a 25 mL round-bottom flask 2-quinolinecarboxaldehyde (413 mg, 2.63 mmol) was dissolved in 8 mL of methanol. (*1S,2S*)- or (*1R,2R*)-diaminocyclohexane (150 mg, 1.31 mmol) was added to the round bottom flask. After a few minutes, a pale-yellow precipitate was formed. The reaction mixture was stirred at room temperature for 2 hours. The yellow precipitate was collected by filtration and washed with diethyl ether (3 × 25 mL). The resulting solid was dried under vacuum (432 mg, 1.10 mmol, yield: 84%).

(1S,2S)-N^1,N^2-bis(quinolin-2-ylmethylene)cyclohexane-1,2-diimine.

^{1}H NMR (500 MHz, $CDCl_3$): δ 8.51 (s, 2H), 8.07 (s, 4H), 8.03 (d, J = 8.5 Hz, 2H), 7.75 (dd, J = 8.2, 0.6 Hz, 2H), 7.68 – 7.63 (m, 2H), 7.50 (dd, J = 11.0, 3.9 Hz, 2H), 3.65 (p, J = 8.8 Hz, 2H), 1.90 (d, J = 11.6 Hz, 6H), 1.56 (d, J = 9.4 Hz, 2H) ppm.

^{13}C NMR (125 MHz, $CDCl_3$): δ 161.86, 154.92, 147.65, 136.39, 129.57, 129.44, 128.70, 127.63, 127.15, 118.56, 77.27, 77.02, 76.76, 73.86, 32.71, 24.37 ppm.

ESI (*m/z*): 415.20 [*M*+Na]$^+$

(1R,2R)-N^1,N^2-bis(quinolin-2-ylmethylene)cyclohexane-1,2-diimine.

^{1}H NMR (500 MHz, $CDCl_3$): δ 8.51 (s, 2H), 8.07 (s, 4H), 8.03 (d, J = 8.5 Hz, 2H), 7.76 – 7.73 (m, 2H), 7.66 (ddd, J = 8.4, 6.9, 1.4 Hz, 2H), 7.49 (ddd, J = 8.1, 6.9, 1.1 Hz, 2H), 3.68 – 3.62 (m, 2H), 1.95 – 1.83 (m, 6H), 1.60 – 1.52 (m, 2H) ppm.

^{13}C NMR (125 MHz, $CDCl_3$): δ 161.87, 154.92, 147.65, 136.42, 129.59, 129.44, 128.71, 127.65, 127.17, 118.57, 77.29, 77.04, 76.78, 73.88, 32.72, 24.38, 0.02 ppm.

ESI (*m/z*): 415.20 [*M*+Na]$^+$

2.2 Synthesis of (1S,2S)- and (1R,2R)-N^1,N^2-bis(quinolin-2-ylmethyl)cyclohexane-1,2-diamine (L).

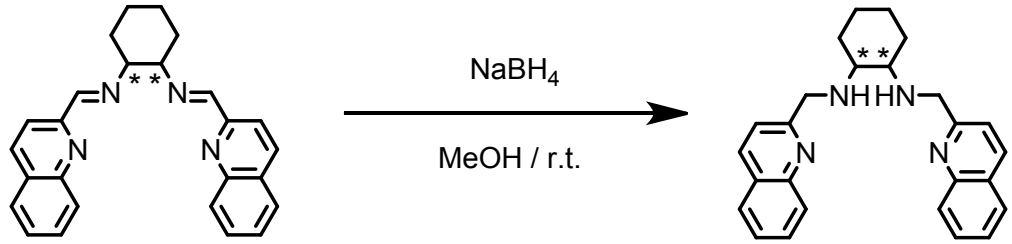

1* **L***

The chiral ligands were synthesized according to a slightly modified literature procedure.[1] The corresponding Schiff base (**1**) (250 mg, 0.637 mmol) was suspended in 60 mL of methanol. Sodium borohydride (128 mg, 3.38 mmol) was added to the reaction mixture portion-wise (4×32 mg) and the solution was stirred for 5 hours at room temperature. As the reaction progressed, the imine starting material dissolved slowly. The solvent was removed under reduced pressure and the residue was taken up with chloroform (3×10 mL). The combined organic fractions were washed with brine and water. The organic phase was dried over $MgSO_4$, filtered and the solvent removed in *vacuo*, yielding a yellow oil (242 mg, 0.610 mmol, yield: 96%).

(1S,2S)-N^1,N^2-bis(quinolin-2-ylmethyl)cyclohexane-1,2-diamine (^{SS}L).

^{1}H NMR (500 MHz, $CDCl_3$) : δ 8.07 (d, J = 8.4 Hz, 2H), 8.03 (d, J = 8.4 Hz, 2H), 7.78 (d, J = 8.1 Hz, 2H), 7.69 – 7.64 (m, 2H), 7.60 (d, J = 8.4 Hz, 2H), 7.50 (t, J = 7.5 Hz, 2H), 4.25 (d, J = 14.6 Hz, 2H), 4.06 (d, J = 14.6 Hz, 2H), 2.57 (s, 2H), 2.42 (dd, J = 5.4, 3.7 Hz, 2H), 2.22 (d, J = 13.2 Hz, 2H), 1.76 – 1.70 (m, 2H), 1.26 (dd, J = 13.2, 6.5 Hz, 2H), 1.12 (d, J = 8.1 Hz, 2H) ppm.

^{13}C NMR (125 MHz, $CDCl_3$): δ 161.26, 147.64, 136.29, 129.30, 128.95, 127.56, 127.30, 125.91, 120.81, 77.28, 77.03, 76.78, 61.66, 53.20, 31.76, 25.02 ppm.

ESI (*m/z*): 397.20 $[M+H]^+$

(1R,2R)-N^1,N^2-bis(quinolin-2-ylmethyl)cyclohexane-1,2-diamine (^{RR}L).

^{1}H NMR (500 MHz, $CDCl_3$): δ 8.08 (d, J = 8.4 Hz, 2H), 8.03 (d, J = 8.5 Hz, 2H), 7.78 (d, J = 8.0 Hz, 2H), 7.67 (dd, J = 11.2, 4.1 Hz, 2H), 7.60 (d, J = 8.4 Hz, 2H), 7.50 (t, J = 7.4 Hz, 2H), 4.26 (d, J = 14.6 Hz, 2H), 4.06 (d, J = 14.6 Hz, 2H), 2.43 (dd, J = 5.2, 3.8 Hz, 2H), 2.22 (d, J = 13.1 Hz, 2H), 1.76 – 1.70 (m, 2H), 1.25 (t, J = 9.8 Hz, 2H), 1.12 (d, J = 8.2 Hz, 2H) ppm.

^{13}C NMR (125 MHz, $CDCl_3$): δ 161.09, 147.59, 136.33, 129.32, 128.91, 127.56, 127.29, 125.93, 120.80, 77.30, 77.04, 76.79, 61.61, 53.10, 31.67, 24.99 ppm.

ESI (*m/z*): 397.20 $[M+H]^+$

***2.3* Synthesis of [(*1S,2S*)- and [(*1R,2R*)-N^1,N^2-bis(quinolino-2-ylmethyl)cyclohexane-1,2-diamino zinc] dinitrate, $[Zn^{SS}L](NO_3)_2$ and $[Zn^{RR}L](NO_3)_2$**

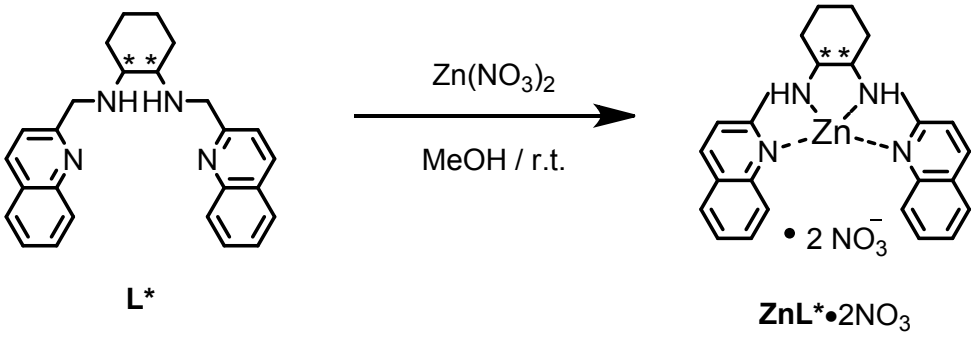

L* **ZnL*•2NO_3**

In a 10 mL round-bottom flask, ^{SS}L or ^{RR}L (120 mg, 0.303 mmol) was dissolved in 7 mL of methanol. Zinc nitrate (90 mg, 0.303 mmol) was dissolved in 0.5 mL ultrapure water in a vial. The two solutions were mixed and stirred overnight. The solution was concentrated in vacuo to ca. 1/3 of the total volume. The residue was mixed with diethyl ether until a precipitate formed. The precipitate was filtered and dried under high vacuum (127 mg, 0.275 mmol, yield: 91%).

[(1S,2S)-N^1,N^2-bis(quinolino-2-ylmethyl)cyclohexane-1,2-diamino zinc] dinitrate, $[Zn^{SS}L](NO_3)_2$

^{1}H NMR (500 MHz, $CDCl_3$) : δ 8.46 (d, J = 8.5 Hz, 2H), 7.93 (d, J = 7.5 Hz, 2H), 7.80 (d, J = 8.7 Hz, 2H), 7.55 (t, J = 7.5 Hz, 2H), 7.52 (d, J = 8.5 Hz, 2H), 7.36 (ddd, J = 8.5, 7.1, 1.3 Hz, 2H), 4.89 (dd, J = 16.9, 6.5 Hz, 2H), 4.58 – 4.51 (m, 2H), 4.28 (dd, J = 16.9, 5.3 Hz, 2H), 2.65 (s, 2H), 2.40 (d, J = 12.9 Hz, 2H), 1.85 (d, J = 8.3 Hz, 2H), 1.46 – 1.36 (m, 2H), 1.31 (t, J = 10.0 Hz, 2H) ppm.

^{13}C NMR (125 MHz, $CDCl_3$): δ 159.05, 144.49, 141.47, 131.88, 128.74, 128.29, 128.00, 126.87, 120.57, 77.28, 77.02, 76.77, 61.63, 50.21, 30.74, 24.46 ppm.

ESI (*m/z*): 522.20 [M+NO_3]$^+$

[(1R,2R)-N^1,N^2-bis(quinolino-2-ylmethyl)cyclohexane-1,2-diamino zinc] dinitrate, $[Zn^{RR}L](NO_3)_2$

^{1}H NMR (500 MHz, $CDCl_3$) : δ 8.46 (d, J = 8.5 Hz, 2H), 7.93 (dd, J = 8.1, 0.9 Hz, 2H), 7.80 (d, J = 8.7 Hz, 2H), 7.57 – 7.53 (m, 2H), 7.52 (d, J = 8.5 Hz, 2H), 7.38 – 7.34 (m, 2H), 4.89 (dd, J = 16.9, 6.5 Hz, 2H), 4.55 (s, 2H), 4.28 (dd, J = 16.9, 5.3 Hz, 2H), 2.69 – 2.60 (m, 2H), 2.40 (d, J = 13.1 Hz, 2H), 1.85 (d, J = 8.3 Hz, 2H), 1.46 – 1.37 (m, 2H), 1.30 (t, J = 10.0 Hz, 2H) ppm.

^{13}C NMR (125 MHz, $CDCl_3$): δ 159.04, 144.47, 141.46, 131.87, 128.73, 128.28, 128.00, 126.87, 120.56, 77.28, 77.02, 76.77, 61.61, 50.20, 30.73, 24.45 ppm.

ESI (*m/z*): 522.20 [M+NO_3]$^+$

2.4 **Synthesis of [(*1R,2R*)-N^1,N^2-bis(quinolino-2-ylmethyl)cyclohexane-1,2-diamino copper(II)] bis(trifluoromethansulfonate), [Cu^{RR}L](CF$_3$SO$_3$)$_2$**

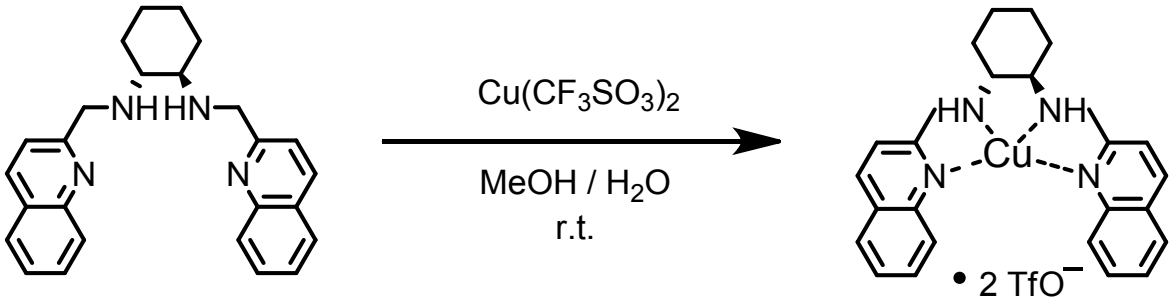

^{RR}**L** **[Cu^{RR}L]**(TfO)$_2$

In a 10 mL round-bottom flask, ^{RR}L (134 mg, 0.338 mmol) was dissolved in 7 mL of methanol. Copper (II) trifluoromethanesulfonate (122 mg, 0.338 mmol) was dissolved in 0.5 mL ultrapure water in a vial. The two solutions were mixed and stirred under nitrogen for 12 hours. The solution was concentrated in vacuo to ca. 1/3 of the total volume. The residue was mixed with diethyl ether until a precipitate formed. The precipitate was filtered and dried under high vacuum (147 mg, 0.319 mmol, yield: 95%).

ESI (m/z): $[M]^+$ 608.11

3. NMR spectra

Figure S1. ^{1}H NMR (500 MHz) of (*1S,2S*)-*N*^{1},*N*^{2}-bis(quinolin-2-ylmethylene)cyclohexane-1,2-diimine in $CDCl_3$

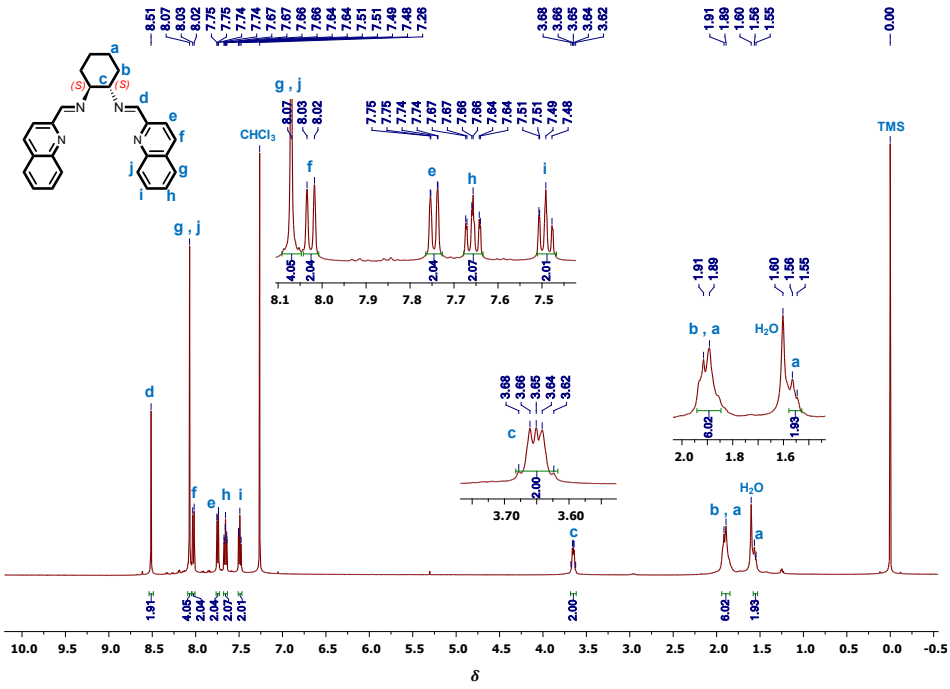

Figure S2. ^{13}C NMR (125 MHz) of (*1S,2S*)-*N*^{1},*N*^{2}-bis(quinolin-2-ylmethylene)cyclohexane-1,2-diimine in $CDCl_3$

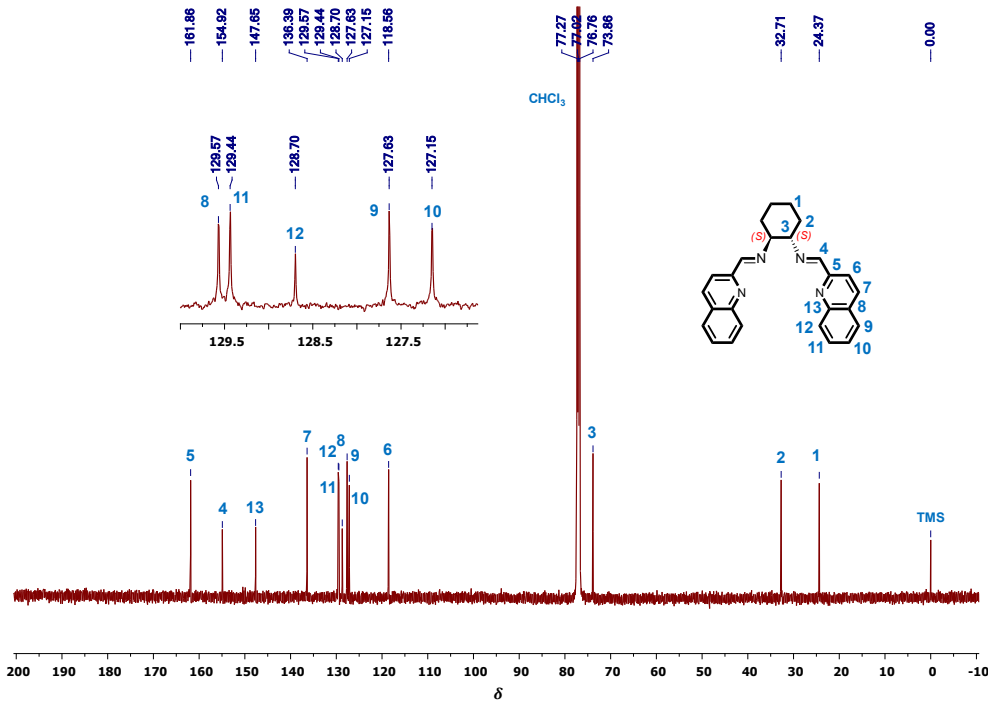

Figure S3. ^{1}H NMR (500 MHz) of (*1R,2R*)-*N*^{1},*N*^{2}-bis(quinolin-2-ylmethylene)cyclohexane-1,2-diimine in $CDCl_3$

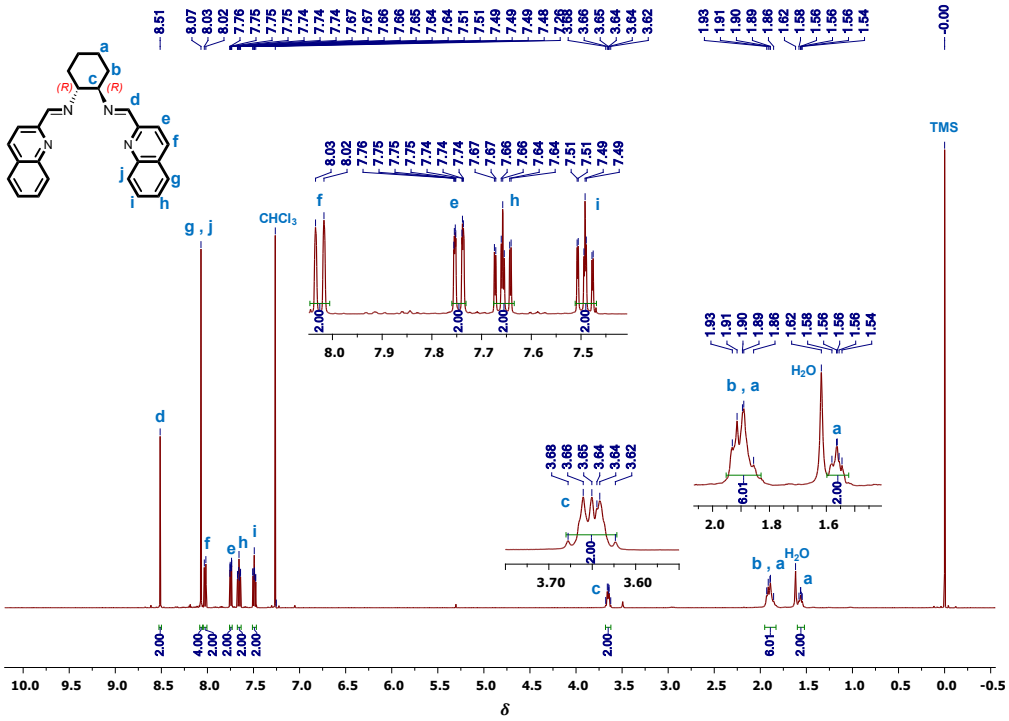

Figure S4. ^{13}C NMR (125 MHz) of (*1R,2R*)-*N*^{1},*N*^{2}-bis(quinolin-2-ylmethylene)cyclohexane-1,2-diimine in $CDCl_3$

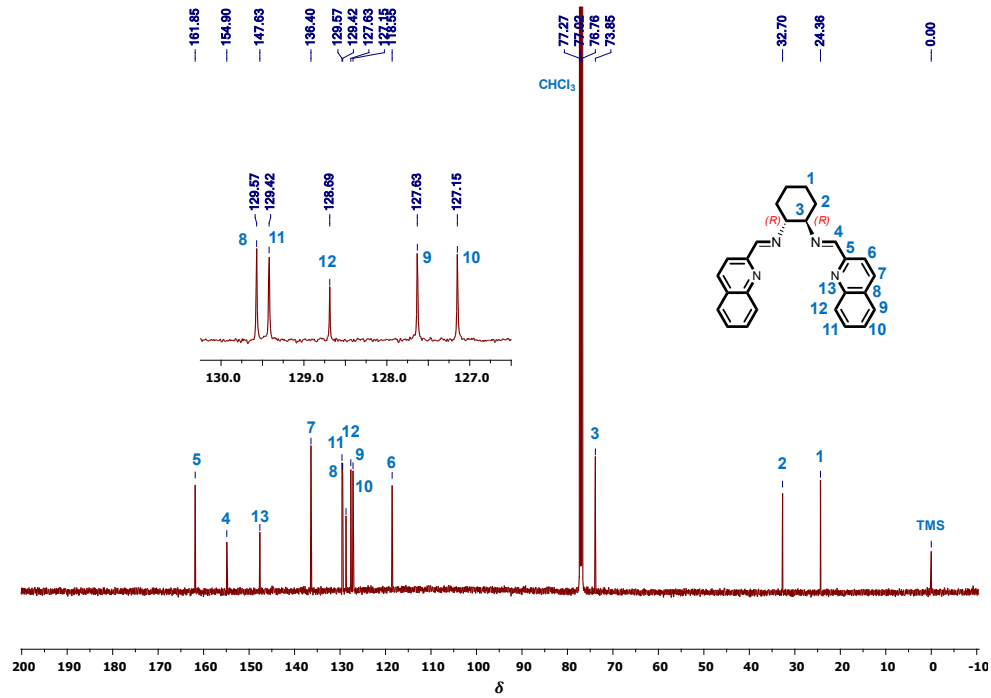

Figure S5. ^{1}H NMR (500 MHz) of ^{SS}L in $CDCl_3$

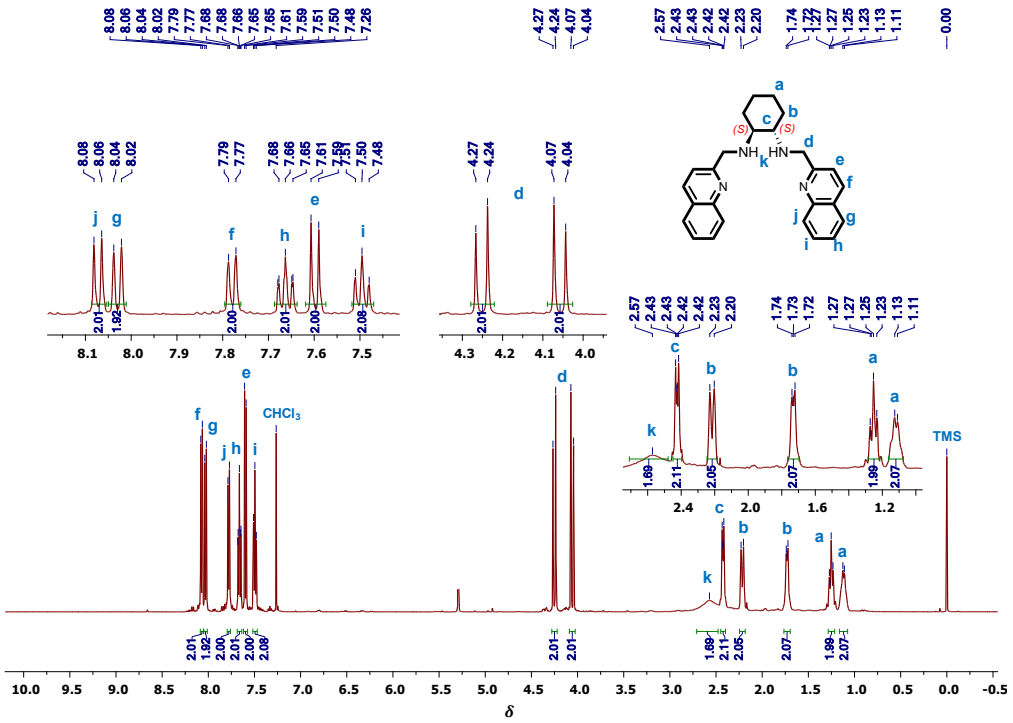

Figure S6. ^{13}C NMR (125 MHz) of ^{SS}L in $CDCl_3$

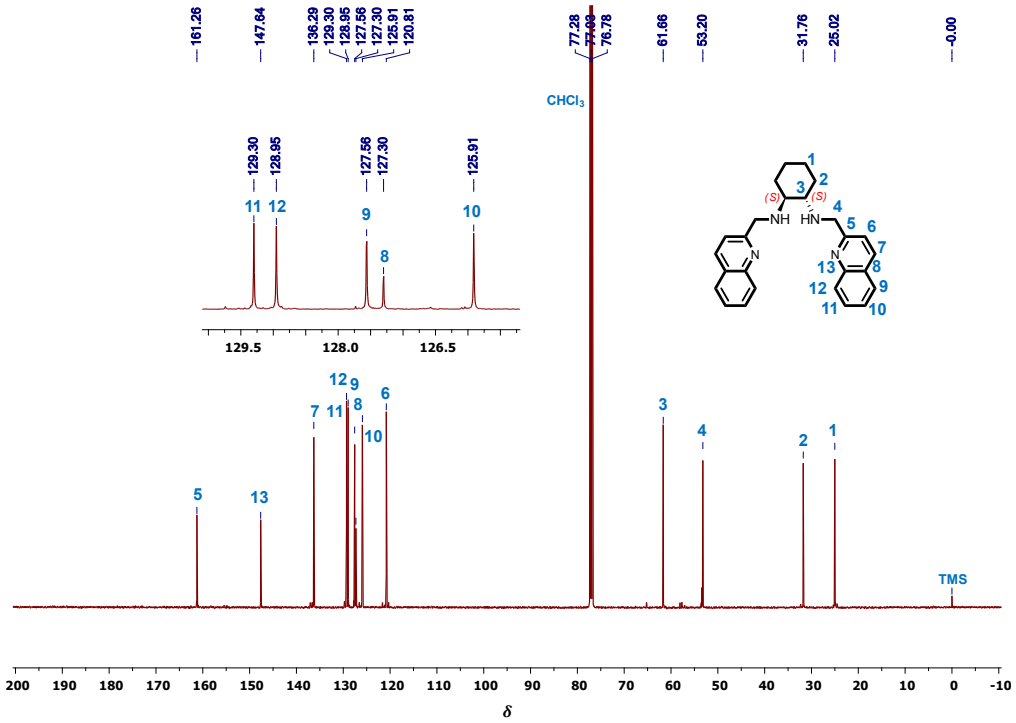

Figure S7. ^{1}H NMR (500 MHz) of ^{RR}L in $CDCl_3$

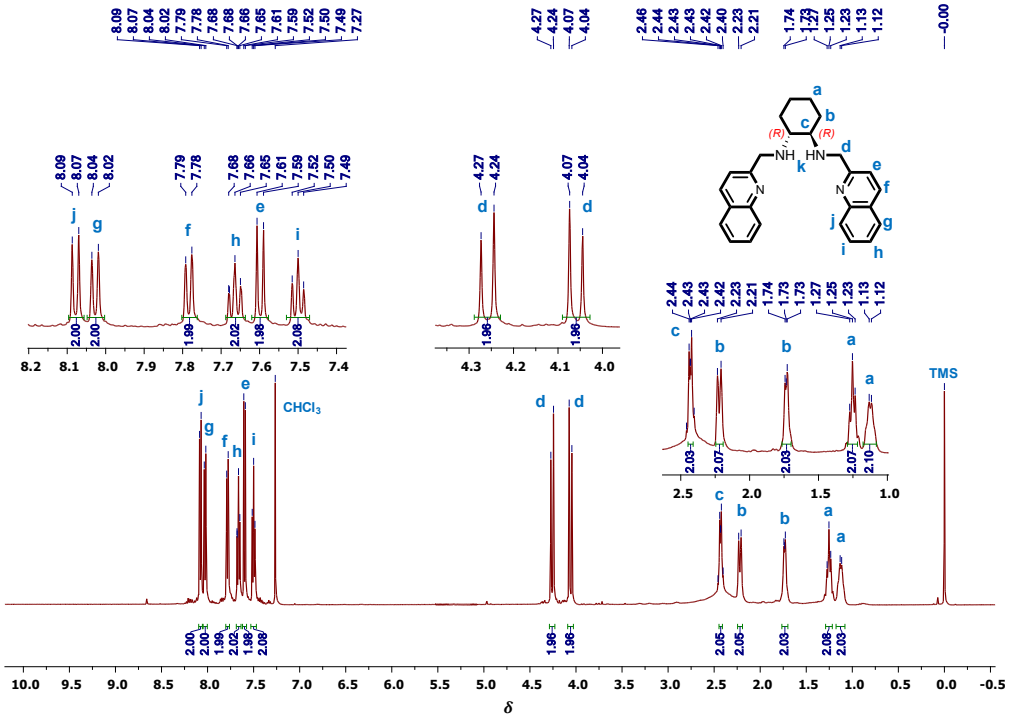

Figure S8. ^{13}C NMR (125 MHz) of ^{RR}L in $CDCl_3$

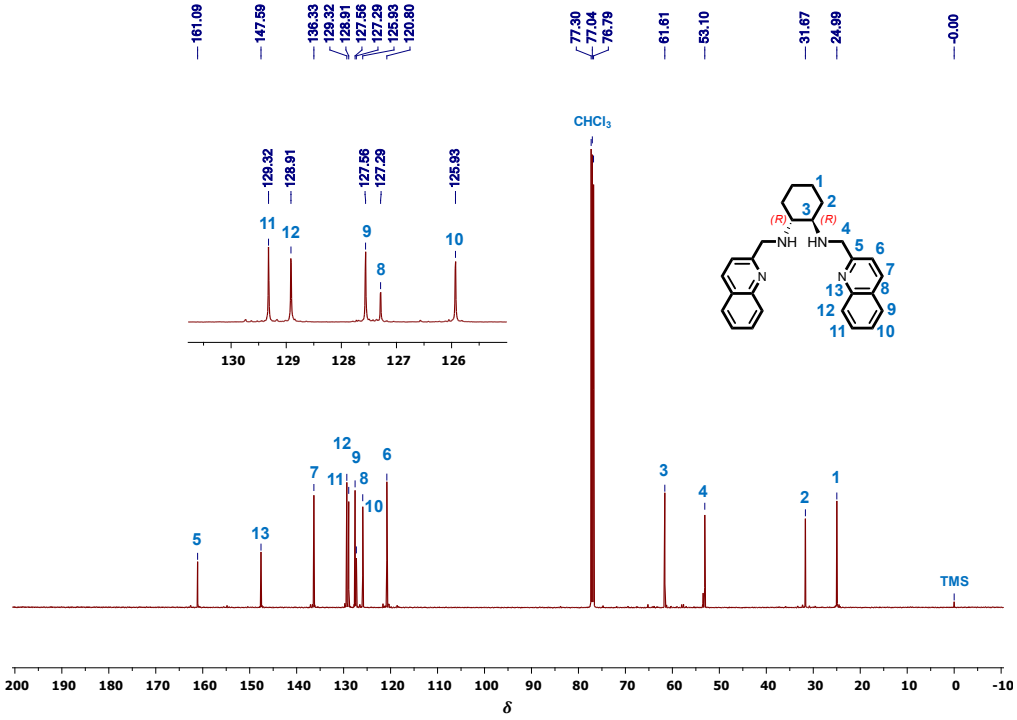

Figure S9. ^{1}H NMR (500 MHz) of [(*1S,2S*)-*N*^{1},*N*^{2}-bis(quinolino-2-ylmethyl)cyclohexane-1,2-diamino zinc] dinitrate, [Zn^{SS}L](NO$_3$)$_2$ in CDCl$_3$

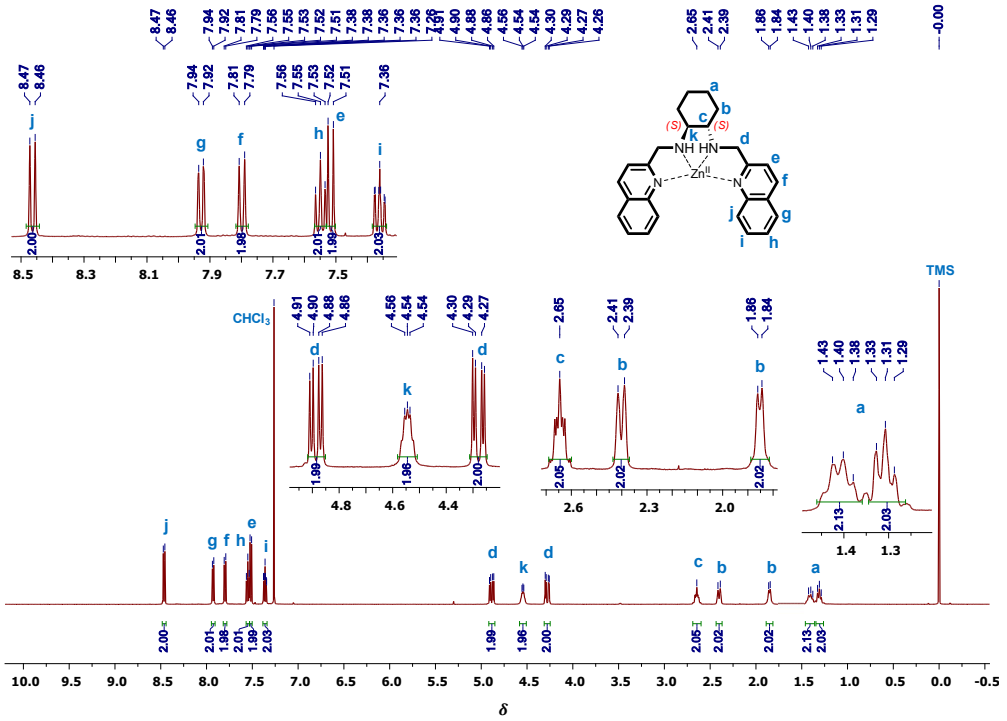

Figure S10. ^{13}C NMR (125 MHz) of [(*1S,2S*)-*N*^{1},*N*^{2}-bis(quinolino-2-ylmethyl)cyclohexane-1,2-diamino zinc] dinitrate, [Zn^{SS}L](NO$_3$)$_2$ in CDCl$_3$

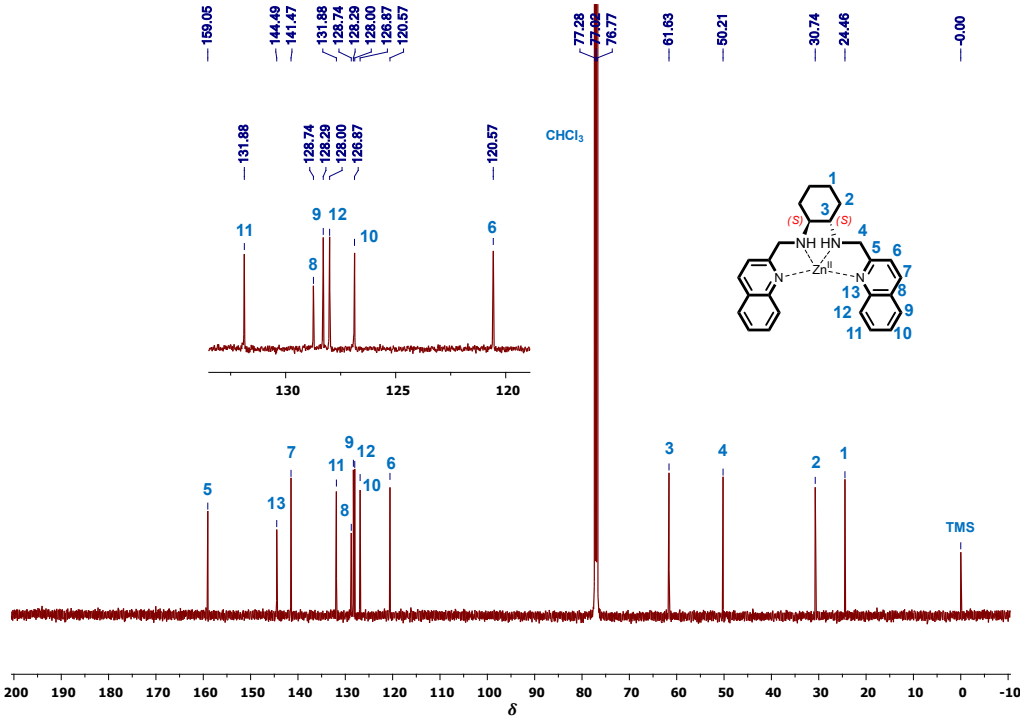

Figure S11. ^{1}H NMR (500 MHz) of [(*1R,2R*)-*N*^{1},*N*^{2}-bis(quinolino-2-ylmethyl)cyclohexane-1,2-diamino zinc] dinitrate, [Zn^{RR}L](NO$_3$)$_2$ in CDCl$_3$

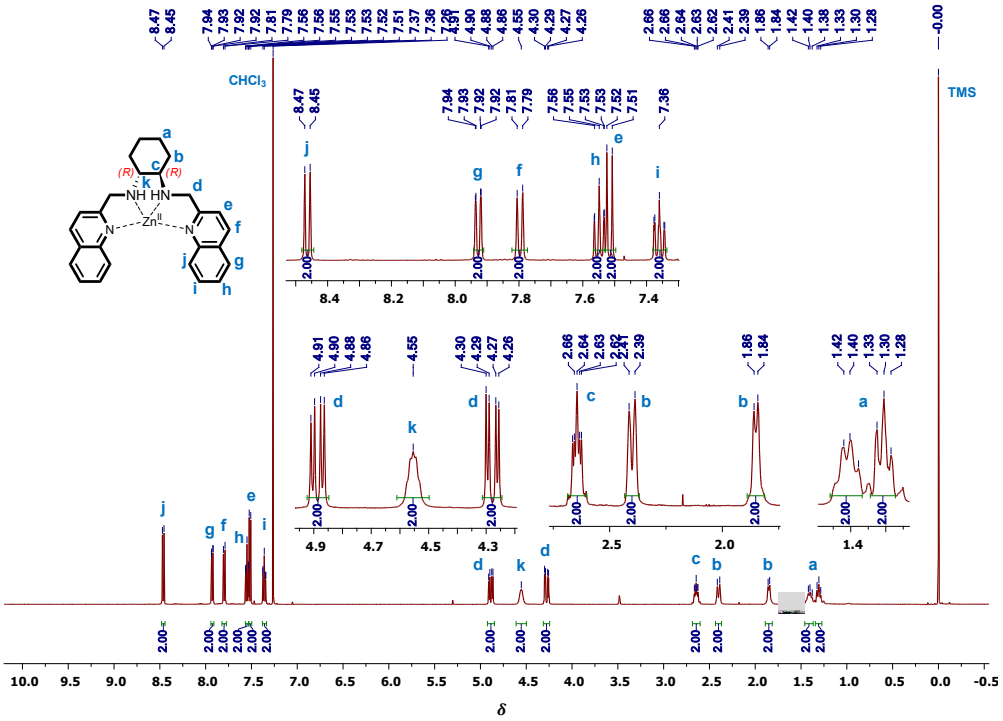

Figure S12. ^{13}C NMR (500 MHz) of [(*1R,2R*)-*N*^{1},*N*^{2}-bis(quinolino-2-ylmethyl)cyclohexane-1,2-diamino] dinitrate, [Zn^{RR}L](NO$_3$)$_2$ in CDCl$_3$

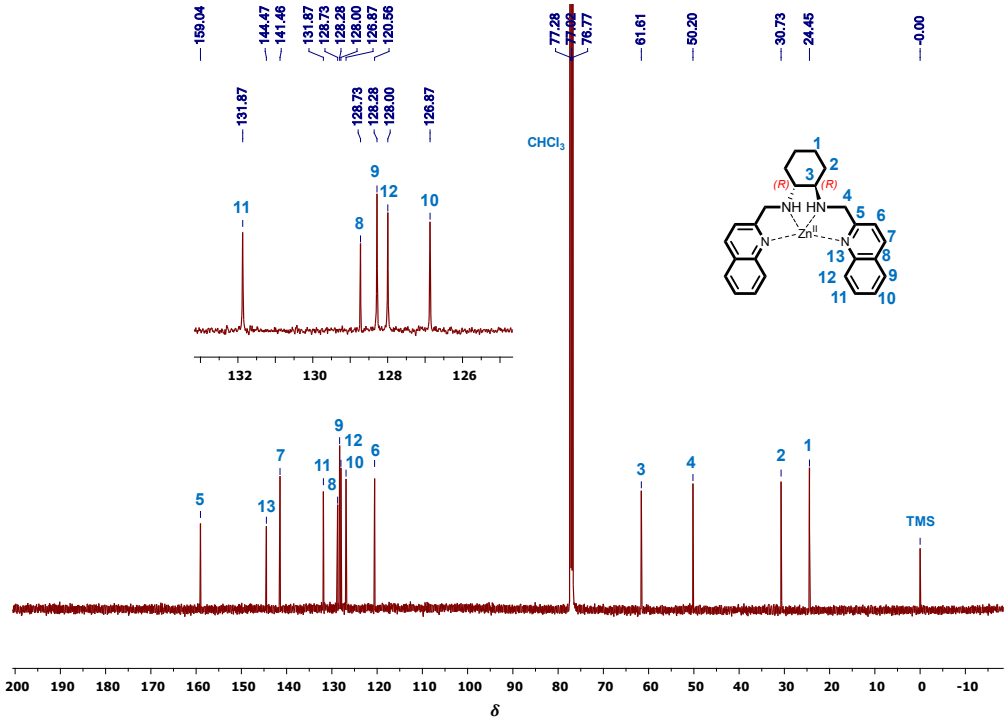

Figure S13. Partial ^{1}H NMR (500 MHz) spectra of ligand ^{RR}L and complex [Zn^{RR}L](NO$_3$)$_2$ in CDCl$_3$

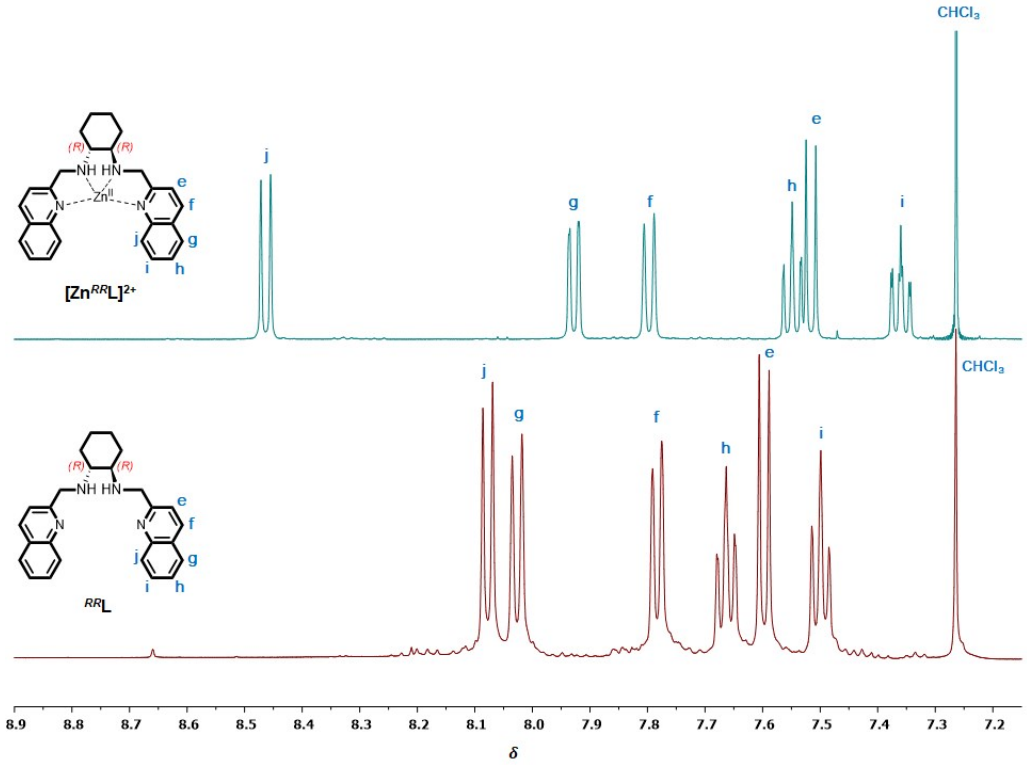

Figure S14. Partial ^{13}C NMR (125 MHz) spectra of ligand ^{RR}L and complex [Zn^{RR}L](NO$_3$)$_2$ in CDCl$_3$

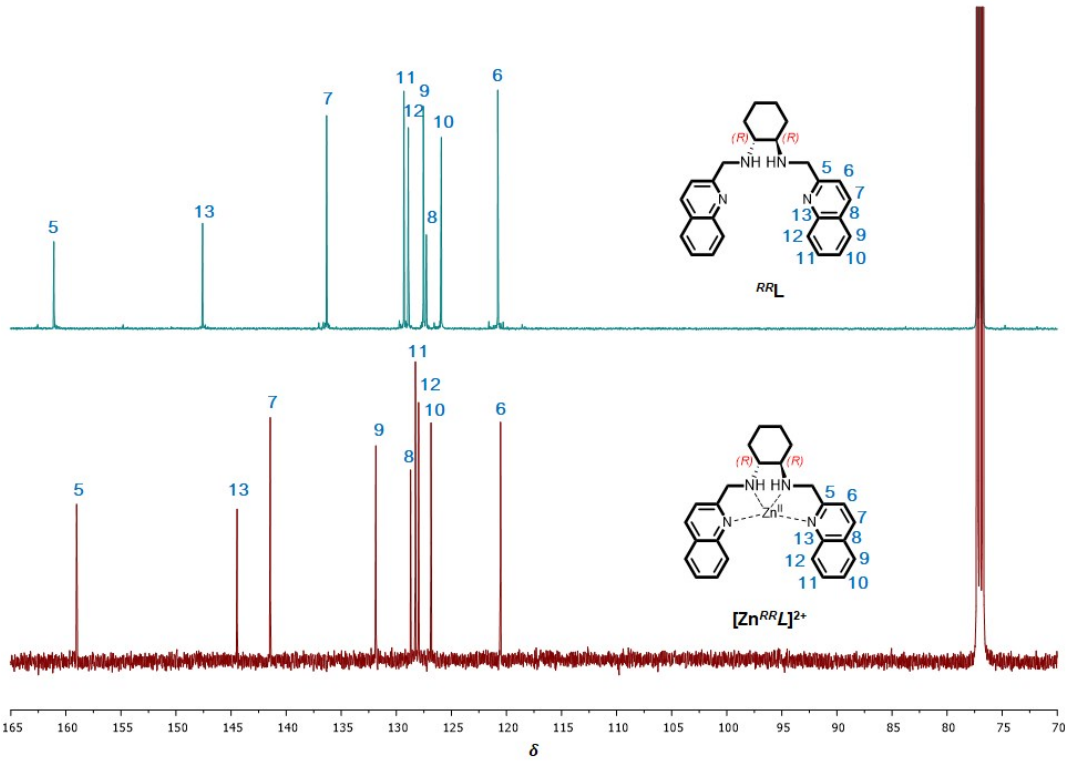

4. Mass Spectra

Figure S15. (A) ESI mass spectrum of (*1S,2S*)-N^1,N^2-bis(quinolin-2-ylmethylene)cyclohexane-1,2-diimine. (B) Calculated isotope pattern for $\mathbf{C_{26}H_{24}N_4Na}$

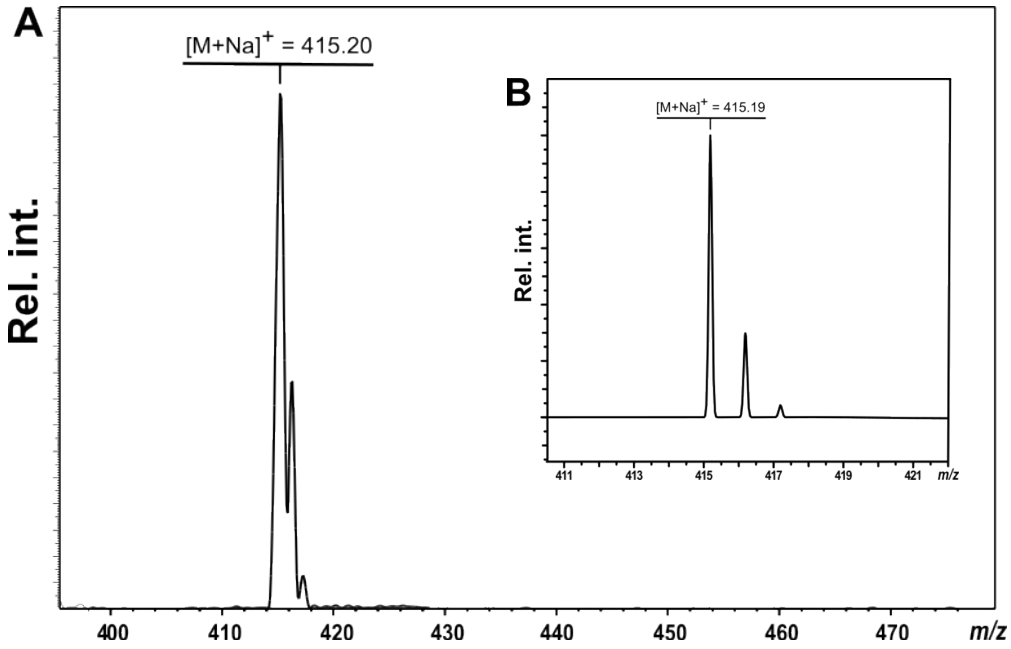

Figure S16. (A) ESI mass spectrum of (*1R,2R*)-N^1,N^2-bis(quinolin-2-ylmethylene)cyclohexane-1,2-diimine. (B) Calculated isotope pattern for $\mathbf{C_{26}H_{24}N_4Na}$

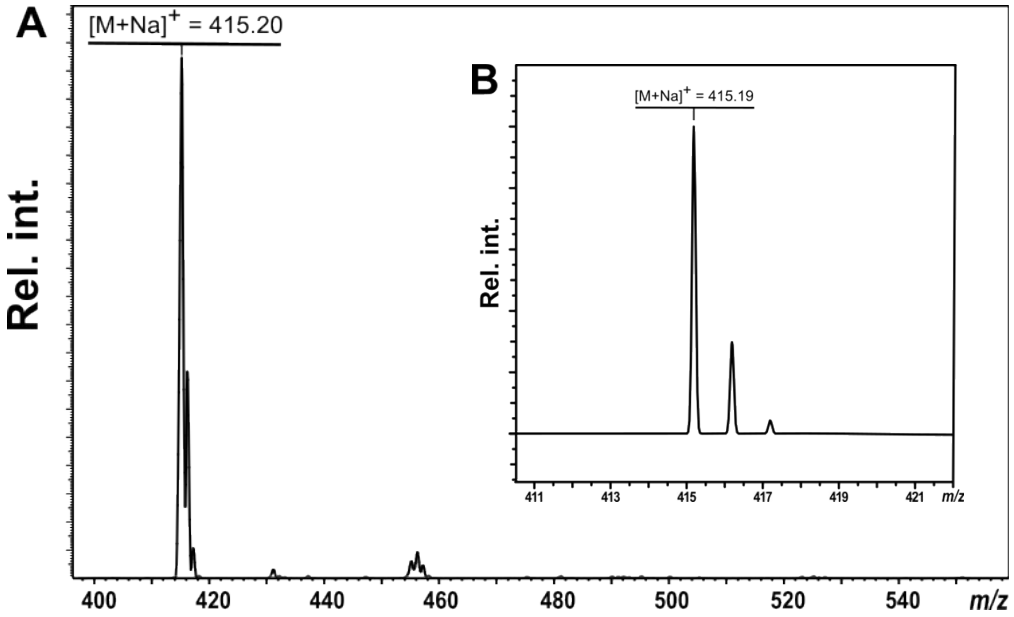

Figure S17. (A) ESI mass spectrum of ^{SS}L. (B) Calculated isotope pattern for $\mathbf{C_{26}H_{29}N_4}$

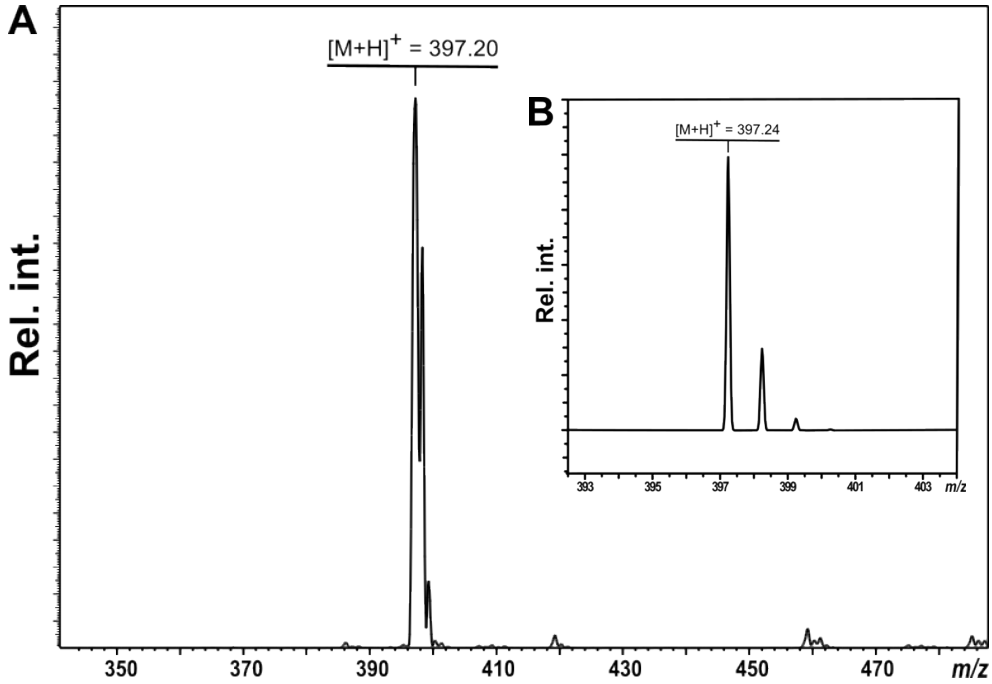

Figure S18. (A) ESI mass spectrum of ^{RR}L. (B) Calculated isotope pattern for $\mathbf{C_{26}H_{29}N_4}$

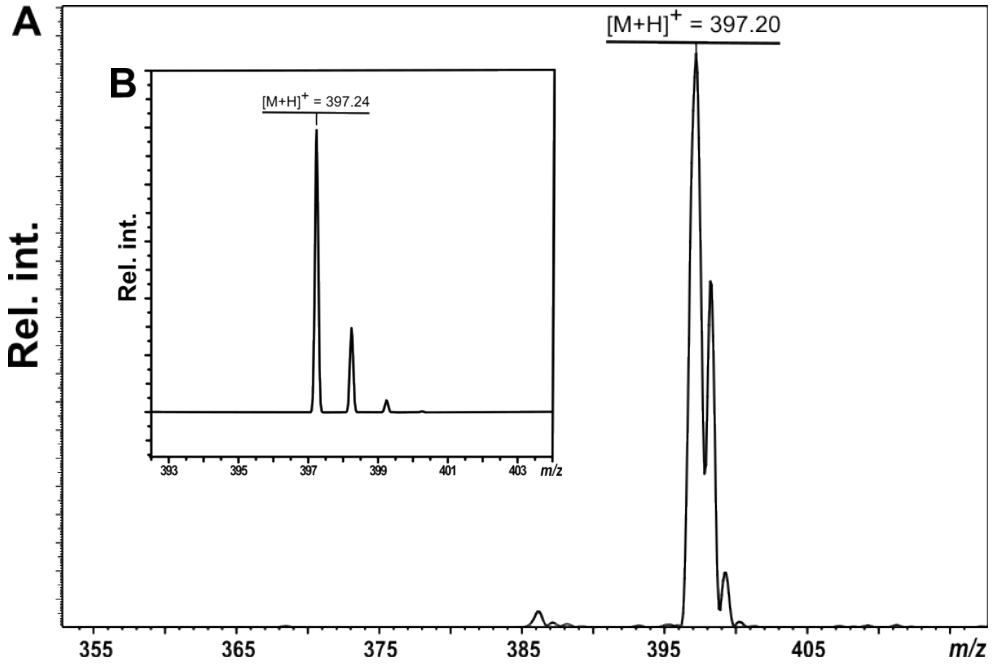

Figure S19. (A) ESI mass spectrum of $[Zn^{SS}L]^{2+}$ (B) Calculated isotope pattern for $\mathbf{C_{26}H_{28}N_5O_3Zn}$

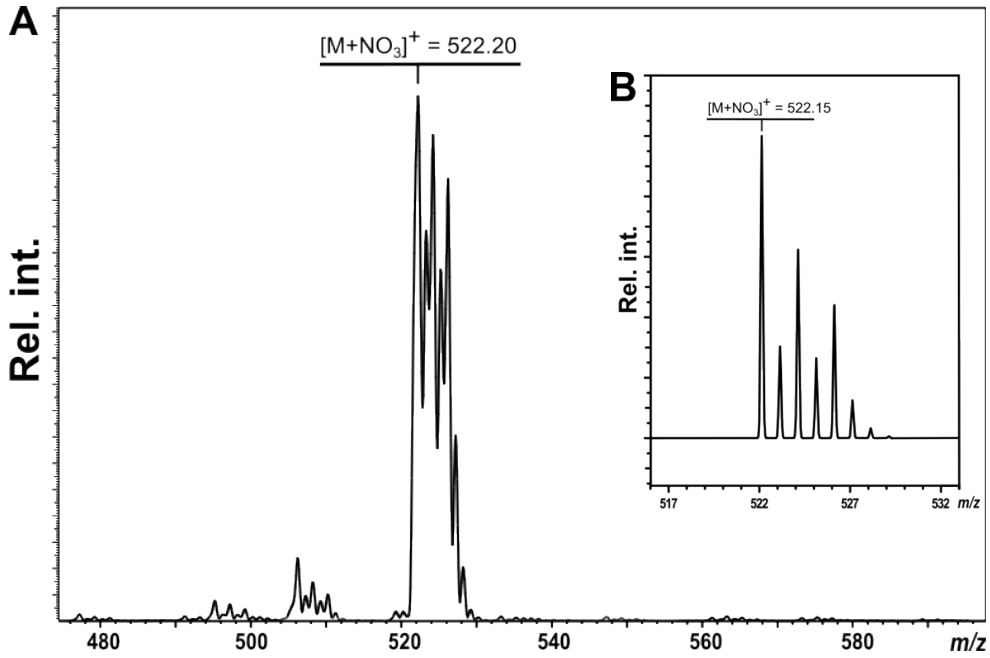

Figure S20. (A) ESI mass spectrum of $[Zn^{RR}L]^{2+}$. (B) Calculated isotope pattern for $\mathbf{C_{26}H_{28}N_5O_3Zn}$

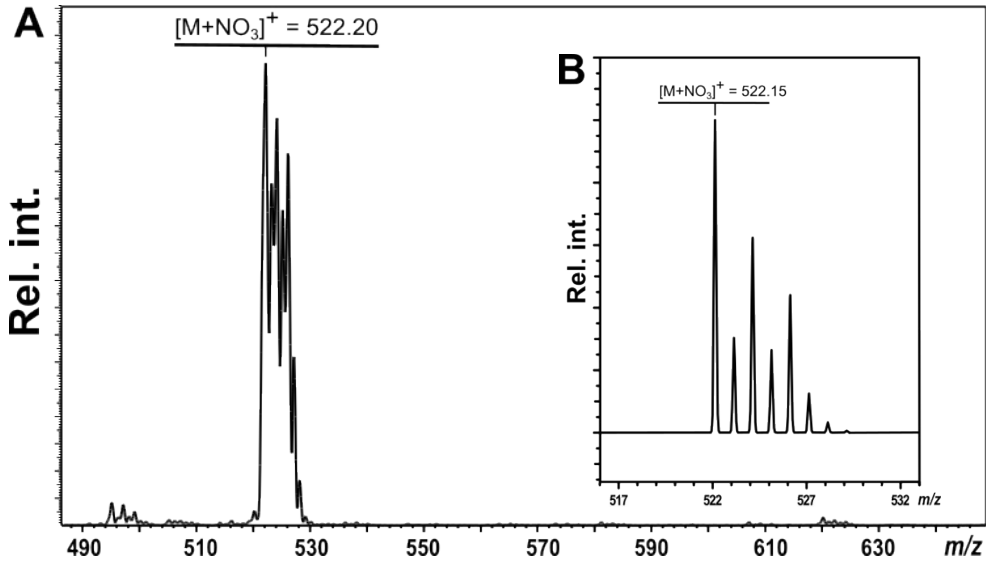

Figure S21. (A) ESI mass spectrum of $[Cu^{RR}L]^{2+}$. (B) Calculated isotope pattern for $\mathbf{C_{27}H_{28}CuF_3N_4O_3S}$

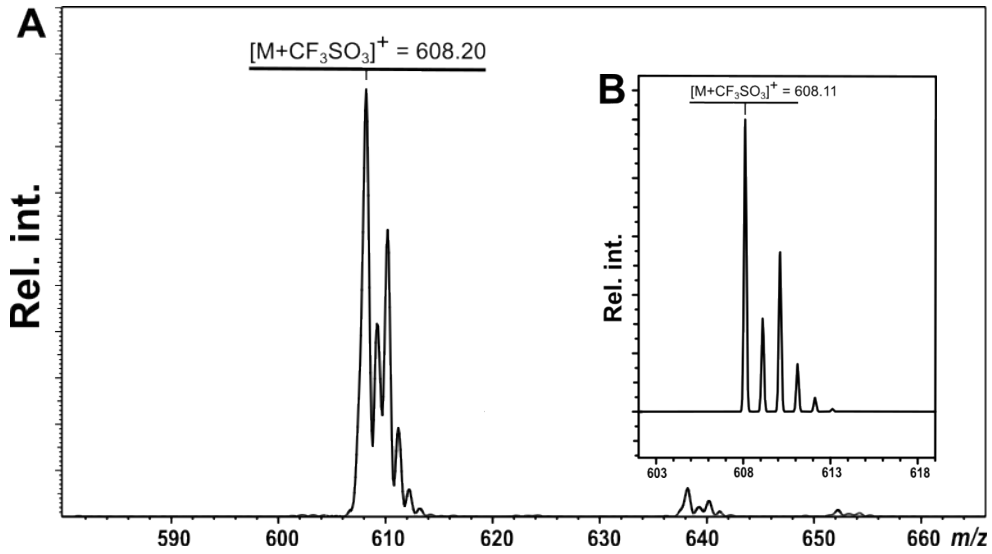

Figure S22. (A) ESI mass spectrum of $[Zn^{RR}L]^{2+}$ and atorvastatin related compound E. (B) Calculated isotope pattern for $\mathbf{C_{59}H_{62}FN_6O_5Zn}$

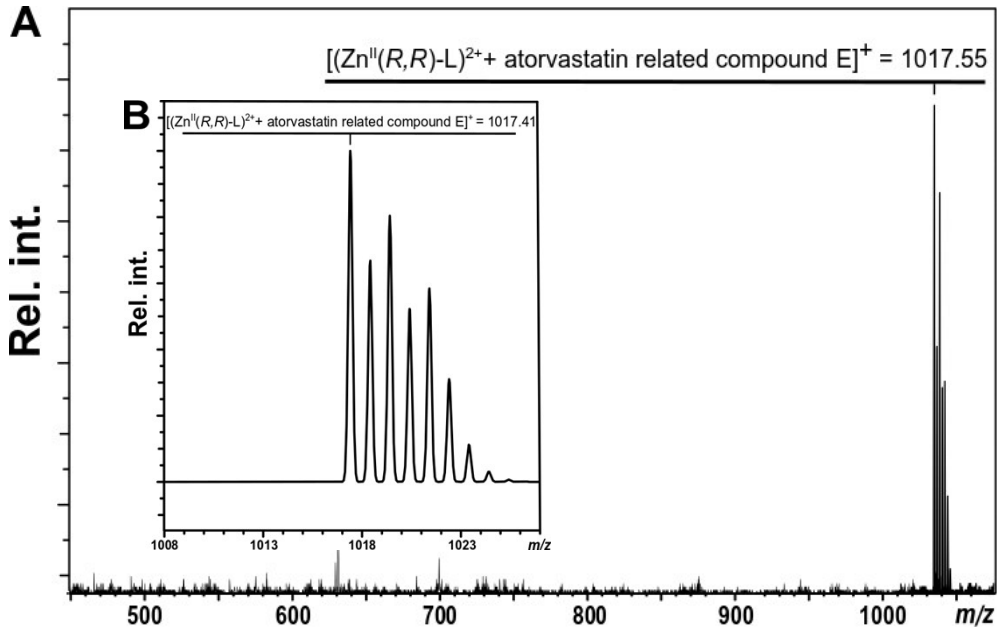

5. Quantum yields and lifetimes of the sensors

Table S1. Photophysical properties of chiral sensors $[Zn^{RR}L]^{2+}$, $[Zn^{SS}L]^{2+}$, and $[Cu^{RR}L]^{2+}$. Absorption maxima ($\lambda_{A,max}$) and fluorescence lifetimes τ_{FL} were acquired in MeCN/H_2O 7:3 solutions buffered to pH = 6 (MES, 50 mM).

Compounds	$\lambda_{A,\,max}$ [nm]	Φ [a] [%]	τ_{FL} [b] [ns]
^{SS}L	274	0.92	
^{RR}L	274	0.92	
$[Cu^{RR}L]^{2+}$	315	0.47	
$[Zn^{RR}L]^{2+}$	315	1.32	8.50 (75.33 %) 27.90 (24.67 %)
$[Zn^{SS}L]^{2+}$	315	1.42	8.50 (83.63 %) 31.90 (16.37 %)

[a] Absolute quantum yields were determined upon excitation at indicated wavelength ($\lambda_{A,\,max}$) for solutions with optical density A < 0.5. All measurements were carried out in non-deoxygenated solutions. [b] The decay profiles of emission were well fitted to the singly exponential decay with χ^2 values less than 1.1

6. Fluorescence titrations

$[Zn^{RR}L]^{2+}$ – Mandelic acid

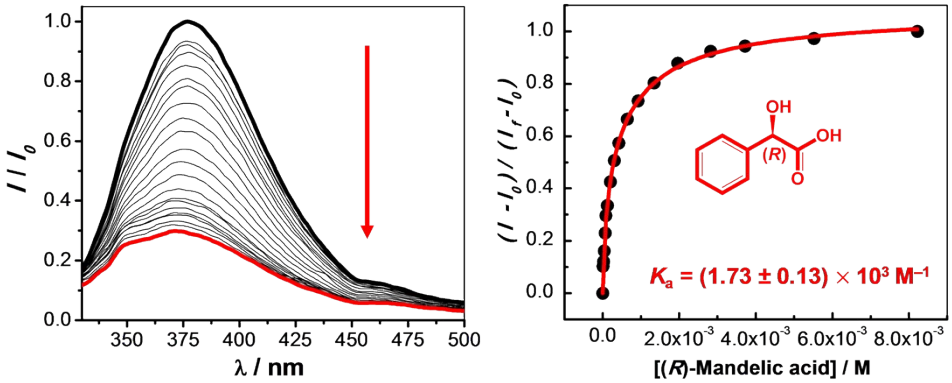

Figure S23. Titration profile and binding isotherm of $[Zn^{RR}L]^{2+}$ (20 μM) with **(*R*)-mandelic acid**. λ_{ex} = 315 nm.

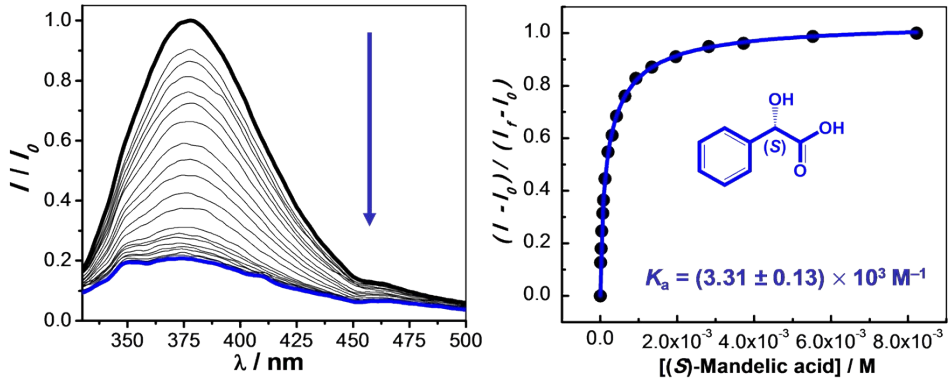

Figure S24. Titration profile and binding isotherm of $[Zn^{RR}L]^{2+}$ (20 μM) with **(*S*)-mandelic acid**. λ_{ex} = 315 nm.

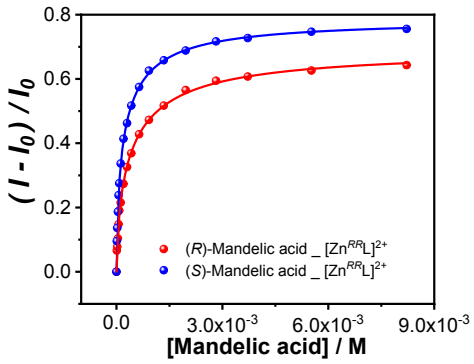

Figure S25. Overlaid binding isotherm of $[Zn^{RR}L]^{2+}$ (20 μM) with **(*R*)-mandelic acid** (red) and **(*S*)-mandelic acid** (blue). λ_{ex} = 315 nm.

$[Zn^{SS}L]^{2+}$ – Mandelic acid

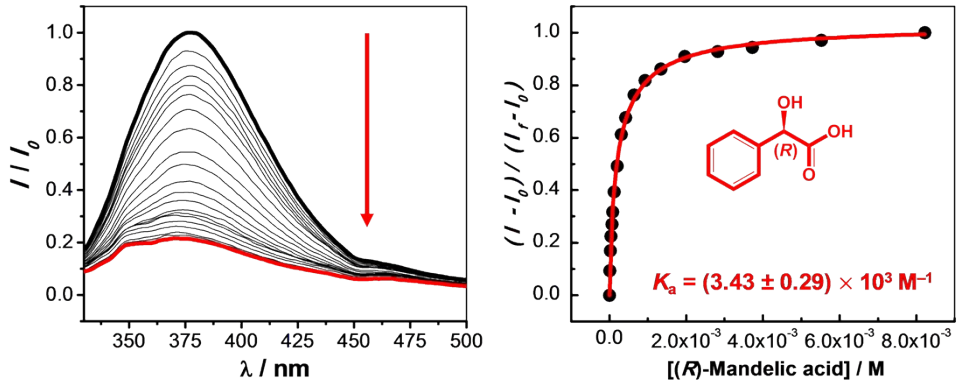

Figure S26. Titration profile and binding isotherm of **$[Zn^{SS}L]^{2+}$** (20 μM) with **(*R*)-mandelic acid**. λ_{ex} = 315 nm.

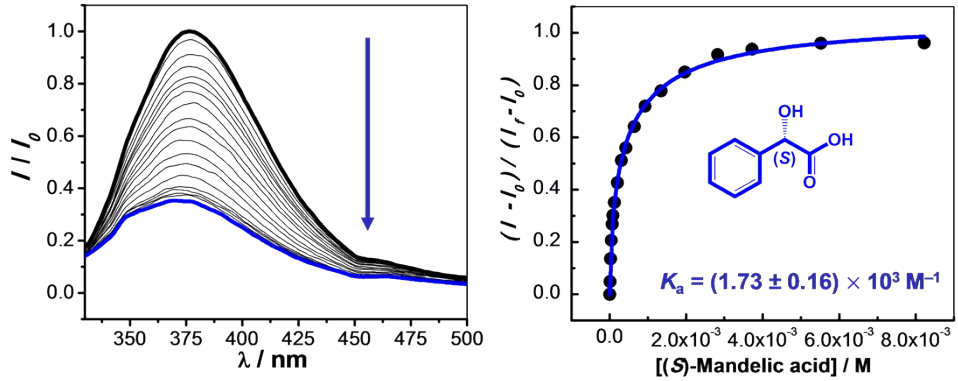

Figure S27. Titration profile and binding isotherm of **$[Zn^{SS}L]^{2+}$** (20 μM) with **(*S*)-mandelic acid**. λ_{ex} = 315 nm.

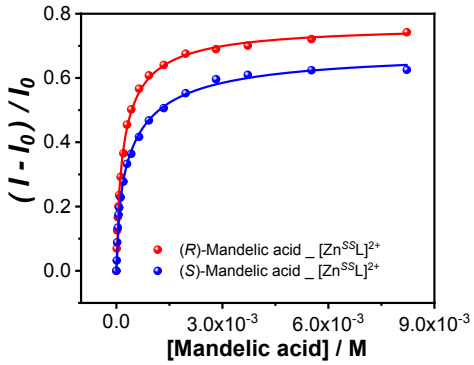

Figure S28. Overlaid binding isotherm of **$[Zn^{SS}L]^{2+}$** (20 μM) with **(*R*)-mandelic acid** (red) and **(*S*)-mandelic acid** (blue). λ_{ex} = 315 nm.

$[Zn^{RR}L]^{2+}$ – Lactic acid

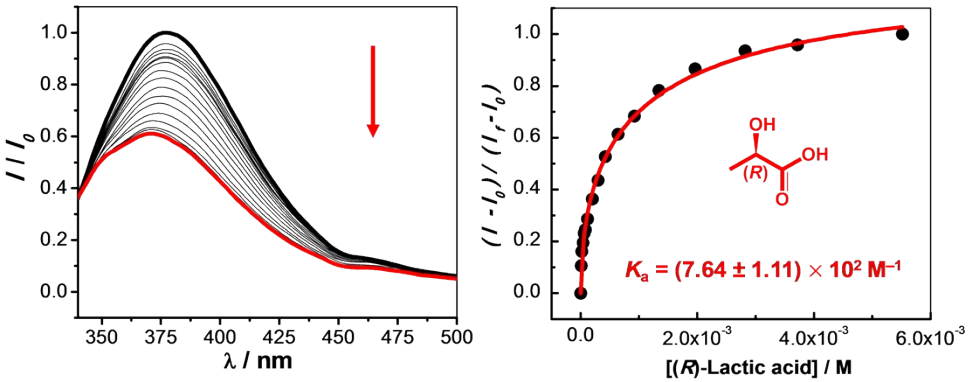

Figure S29. Titration profile and binding isotherm of **$[Zn^{RR}L]^{2+}$** (20 μM) with **(*R*)-lactic acid**. λ_{ex} = 315 nm.

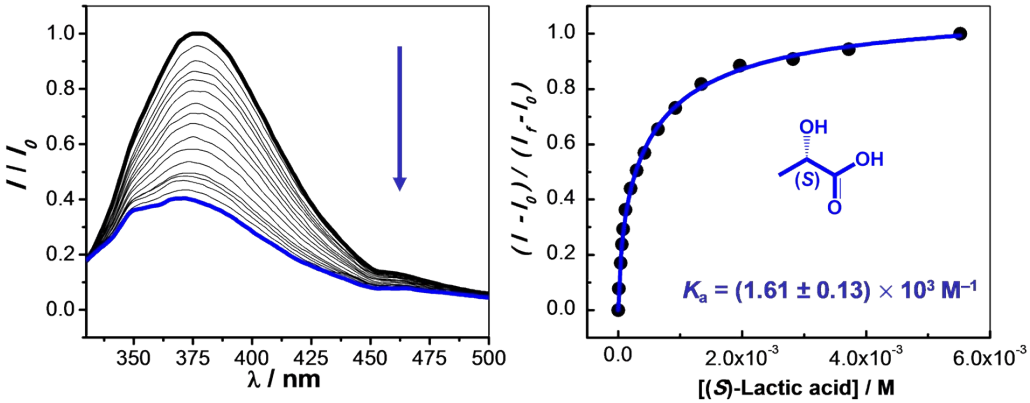

Figure S30. Titration profile and binding isotherm of **$[Zn^{RR}L]^{2+}$** (20 μM) with **(*S*)-lactic acid**. λ_{ex} = 315 nm.

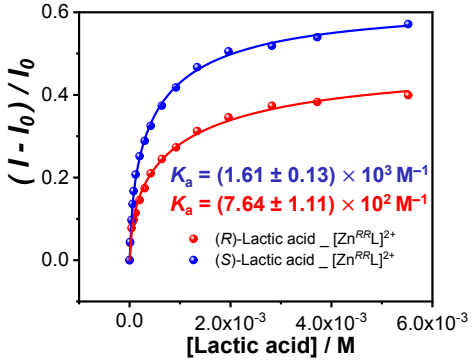

Figure S31. Overlaid binding isotherm of **$[Zn^{RR}L]^{2+}$** (20 μM) with **(*R*)-lactic acid** (red) and **(*S*)-lactic acid** (blue). λ_{ex} = 315 nm.

$[Zn^{SS}L]^{2+}$ – Lactic acid

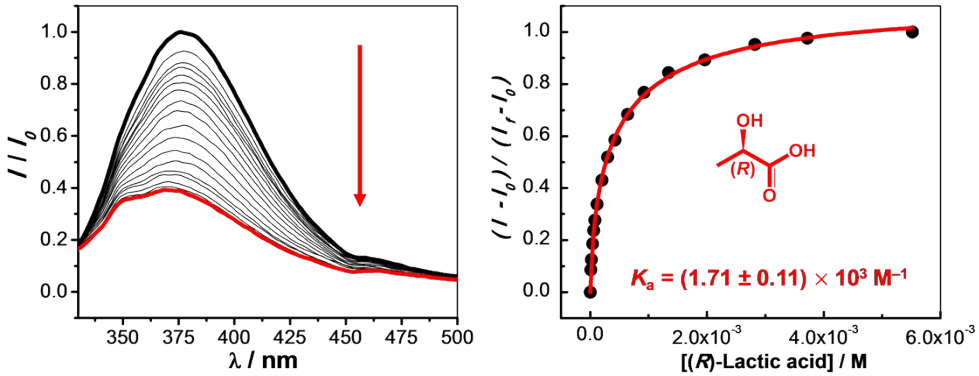

Figure S32. Titration profile and binding isotherm of **$[Zn^{SS}L]^{2+}$** (20 μM) with **(*R*)-lactic acid**. λ_{ex} = 315 nm.

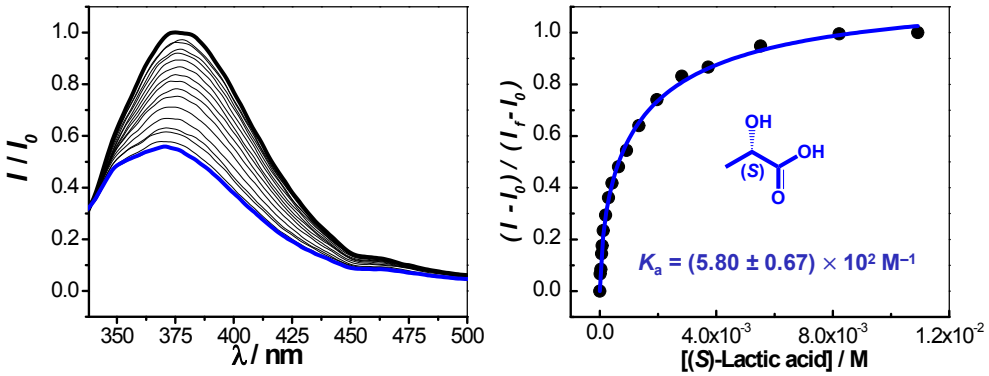

Figure S33. Titration profile and binding isotherm of **$[Zn^{SS}L]^{2+}$** (20 μM) with **(*S*)-lactic acid**. λ_{ex} = 315 nm.

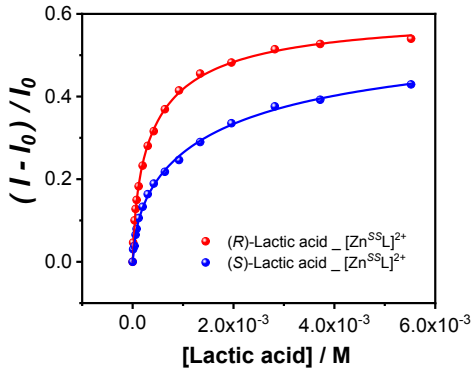

Figure S34. Overlaid binding isotherm of **$[Zn^{SS}L]^{2+}$** (20 μM) with **(*R*)-lactic acid** (red) and **(*S*)-lactic acid** (blue). λ_{ex} = 315 nm.

$[Zn^{RR}L]^{2+}$ – 2-Hydroxy-3-methylbutanoic acid

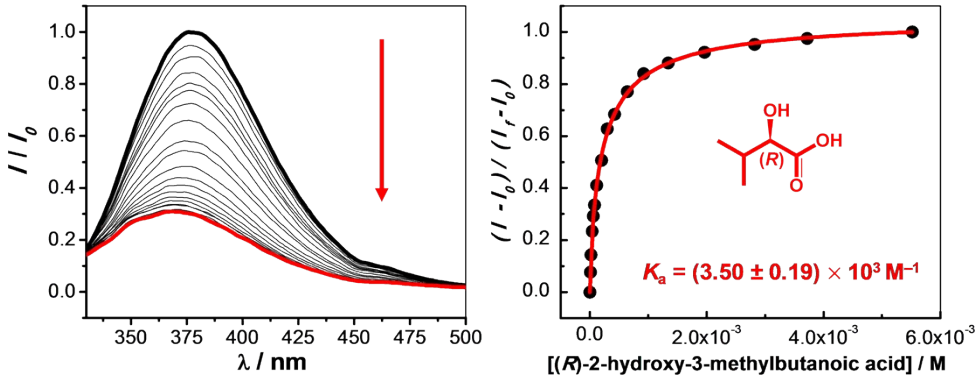

Figure S35. Titration profile and binding isotherm of $[Zn^{RR}L]^{2+}$ (20 μM) with **(*R*)-2-hydroxy-3-methylbutanoic acid**. λ_{ex} = 315 nm.

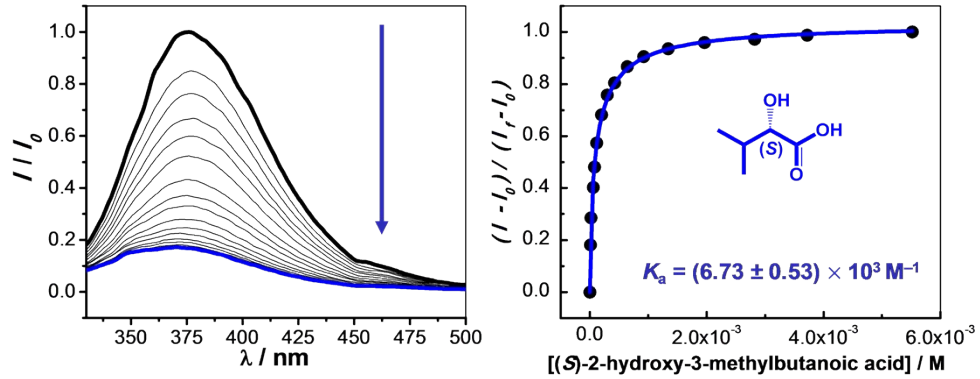

Figure S36. Titration profile and binding isotherm of $[Zn^{RR}L]^{2+}$ (20 μM) with **(*S*)-2-hydroxy-3-methylbutanoic acid**. λ_{ex} = 315 nm.

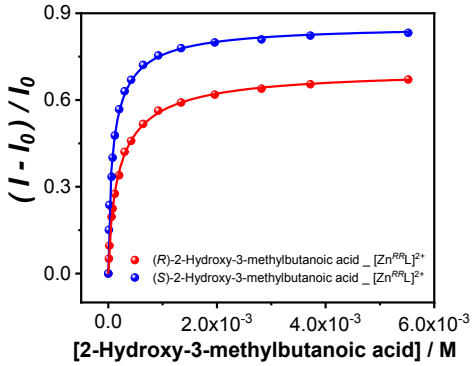

Figure S37. Overlaid binding isotherm of $[Zn^{RR}L]^{2+}$ (20 μM) with **(*R*)-2-hydroxy-3-methylbutanoic acid** (red) and **(*S*)-2-hydroxy-3-methylbutanoic acid** (blue). λ_{ex} = 315 nm.

$[Zn^{SS}L]^{2+}$ – 2-Hydroxy-3-methylbutanoic acid

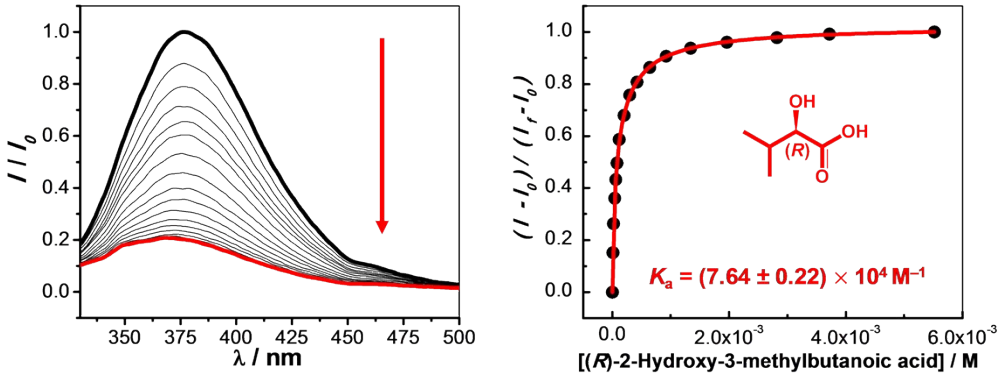

Figure S38. Titration profile and binding isotherm of $[Zn^{SS}L]^{2+}$ (20 μM) with **(*R*)-2-hydroxy-3-methylbutanoic acid**. λ_{ex} = 315 nm.

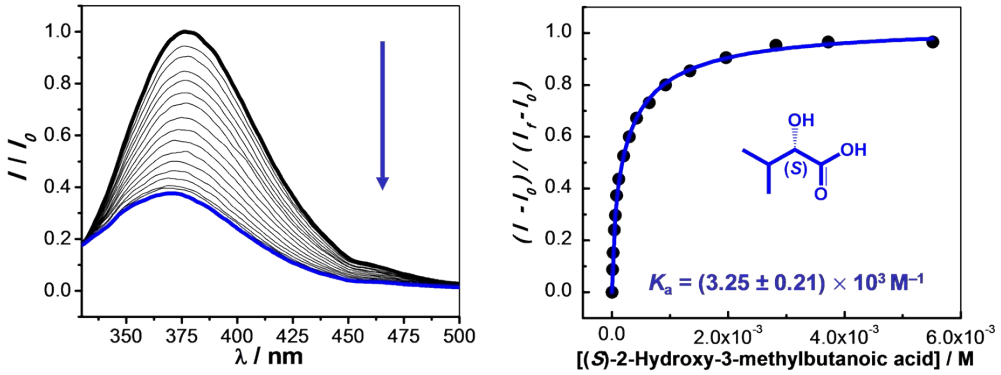

Figure S39. Titration profile and binding isotherm of $[Zn^{SS}L]^{2+}$ (20 μM) with **(*S*)-2-hydroxy-3-methylbutanoic acid**. λ_{ex} = 315 nm.

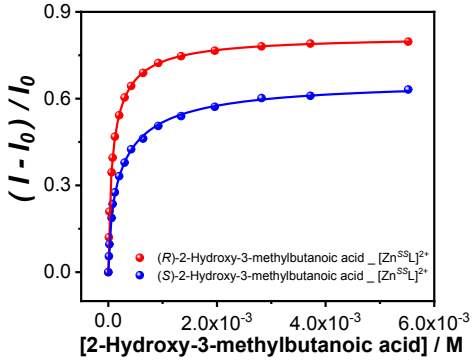

Figure S40. Overlaid binding isotherm of $[Zn^{SS}L]^{2+}$ (20 μM) with **(*R*)-2-hydroxy-3-methylbutanoic acid** (red) and **(*S*)-2-hydroxy-3-methylbutanoic acid** (blue). λ_{ex} = 315 nm.

$[Zn^{RR}L]^{2+}$ – 3-phenyllactic acid

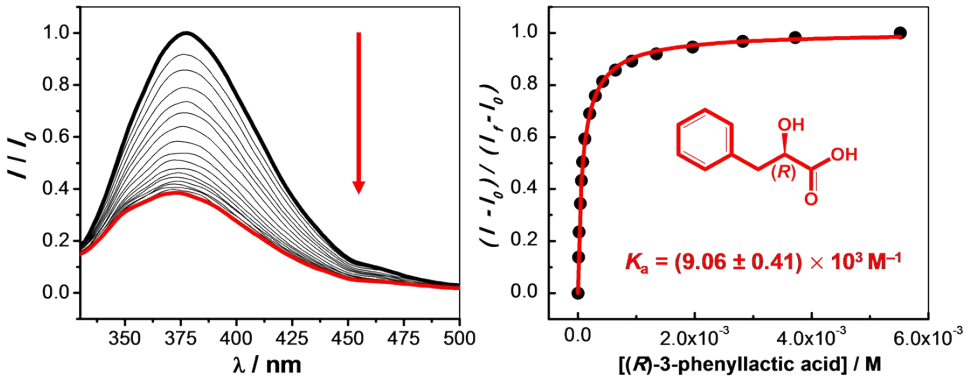

Figure S41. Titration profile and binding isotherm of **$[Zn^{RR}L]^{2+}$** (20 μM) with **(*R*)-3-phenyllactic acid**. λ_{ex} = 315 nm.

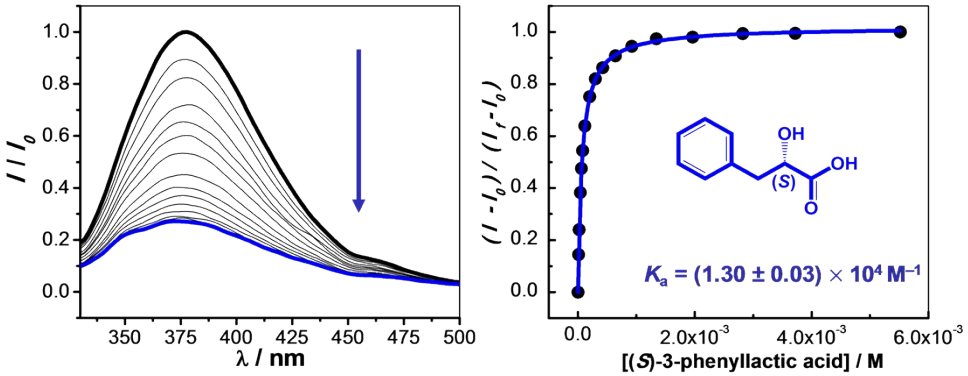

Figure S42. Titration profile and binding isotherm of **$[Zn^{RR}L]^{2+}$** (20 μM) with **(*S*)-3-phenyllactic acid**. λ_{ex} = 315 nm.

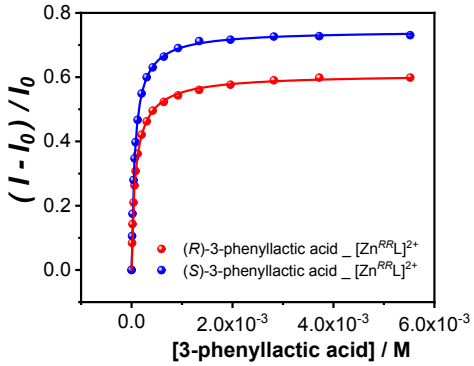

Figure S43. Overlaid binding isotherm of **$[Zn^{RR}L]^{2+}$** (20 μM) with **(*R*)-3-phenyllactic acid** (red) and **(*S*)-3-phenyllactic acid** (blue). λ_{ex} = 315 nm.

$[Zn^{SS}L]^{2+}$ – 3-phenyllactic acid

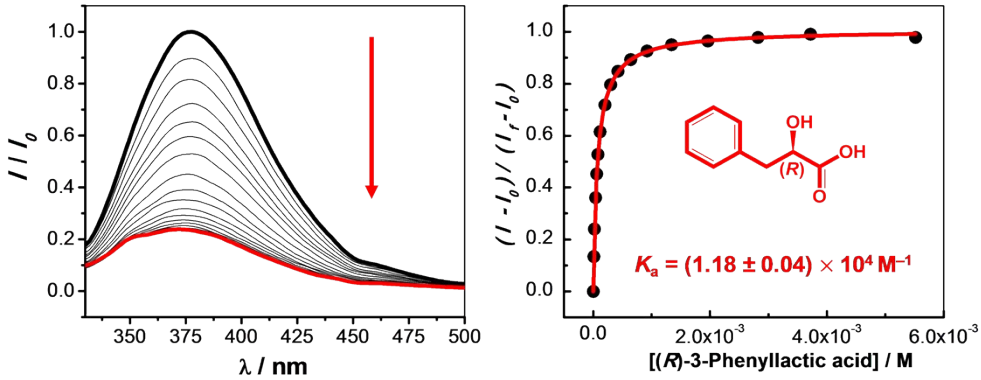

Figure S44. Titration profile and binding isotherm of **$[Zn^{SS}L]^{2+}$** (20 μM) with **(*R*)-3-phenyllactic acid**. λ_{ex} = 315 nm.

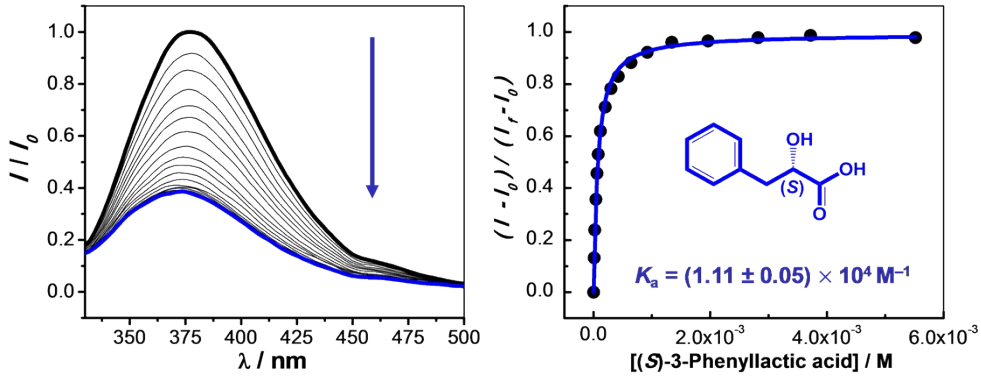

Figure S45. Titration profile and binding isotherm of **$[Zn^{SS}L]^{2+}$** (20 μM) with **(*S*)-3-phenyllactic acid**. λ_{ex} = 315 nm.

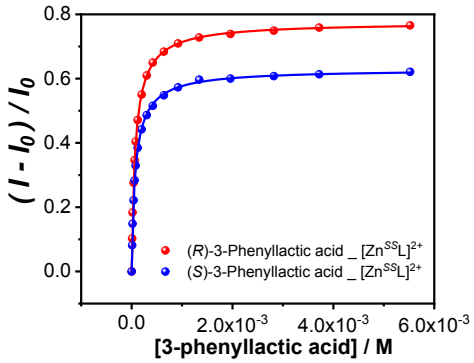

Figure S46. Overlaid binding isotherm of **$[Zn^{SS}L]^{2+}$** (20 μM) with **(*R*)-3-phenyllactic acid** (red) and **(*S*)-3-phenyllactic acid** (blue). λ_{ex} = 315 nm.

$[Zn^{RR}L]^{2+}$ – Atorvastatin

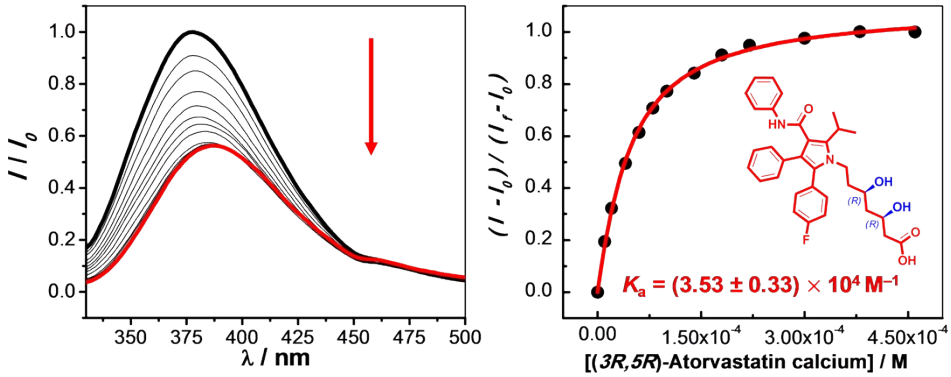

Figure S47. Titration profile and binding isotherm of **$[Zn^{RR}L]^{2+}$** (20 μM) with **(*3R*,*5R*)-atorvastatin calcium**. λ_{ex} = 315 nm.

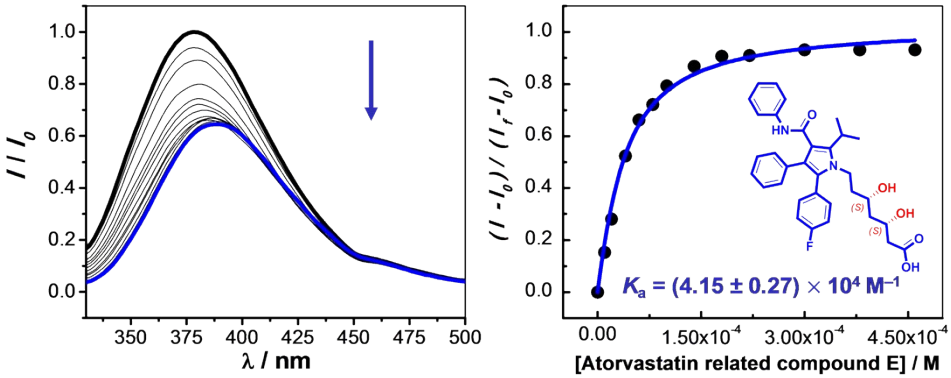

Figure S48. Titration profile and binding isotherm of **$[Zn^{RR}L]^{2+}$** (20 μM) with **(*3S*,*5S*)-atorvastatin related compound E**. λ_{ex} = 315 nm.

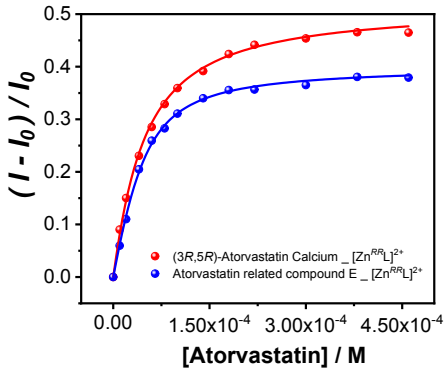

Figure S49. Overlaid binding isotherm of **$[Zn^{RR}L]^{2+}$** (20 μM) with **(*3R*,*5R*)-atorvastatin calcium** (red) and **(*3S*,*5S*)-atorvastatin related compound E**. (blue). λ_{ex} = 315 nm.

$[Zn^{SS}L]^{2+}$ – Atorvastatin

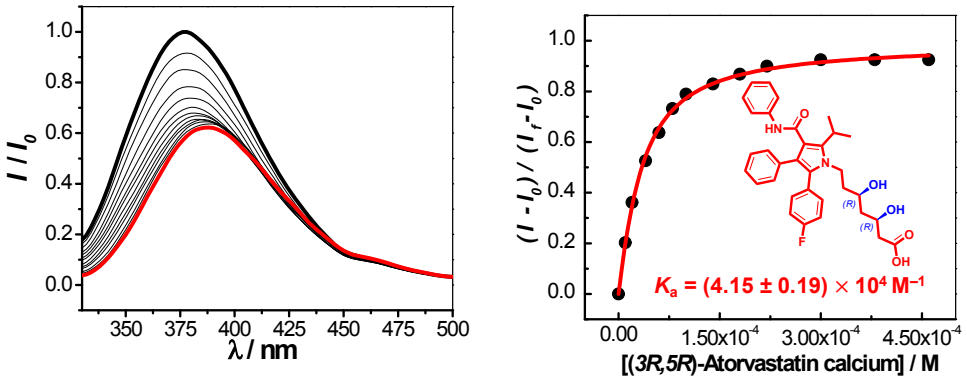

Figure S50. Titration profile and binding isotherm of **$[Zn^{SS}L]^{2+}$** (20 μM) with **(*3R,5R*)-atorvastatin calcium**. λ_{ex} = 315 nm.

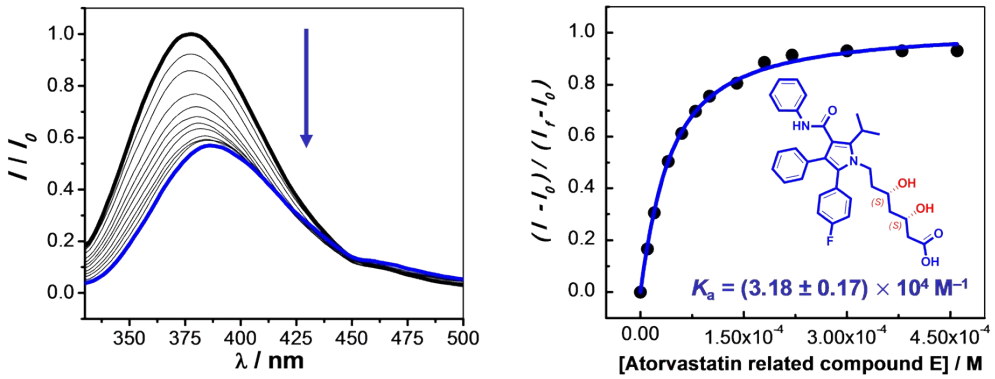

Figure S51. Titration profile and binding isotherm of **$[Zn^{SS}L]^{2+}$** (20 μM) with **(*3S,5S*)-atorvastatin related compound E**. λ_{ex} = 315 nm

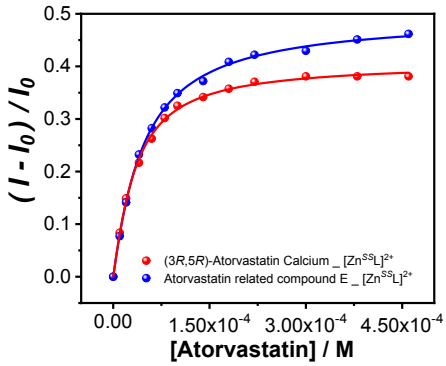

Figure S52. Overlaid binding isotherm of **$[Zn^{SS}L]^{2+}$** (20 μM) with **(*3R,5R*)-atorvastatin calcium** (red) and **(*3S,5S*)-atorvastatin related compound E**. (blue). λ_{ex} = 315 nm.

$[Zn^{RR}L]^{2+}$ – Ibuprofen

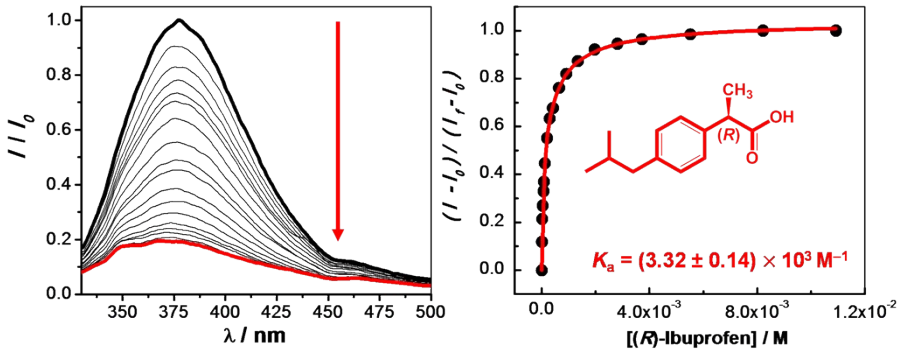

Figure S53. Titration profile and binding isotherm of $[Zn^{RR}L]^{2+}$ (20 μM) with **(*R*)-Ibuprofen**. λ_{ex} = 315 nm.

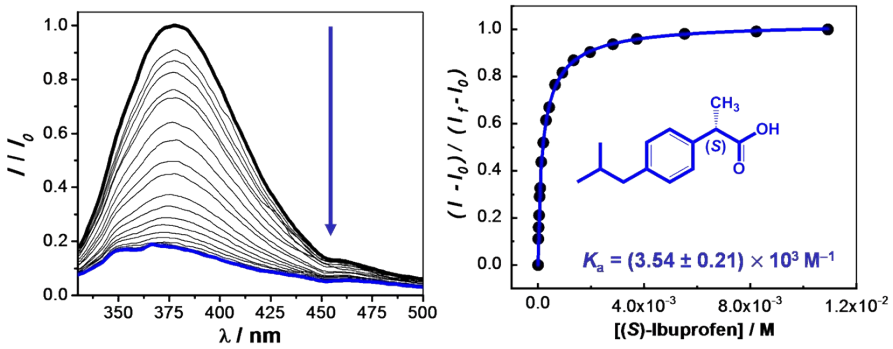

Figure S54. Titration profile and binding isotherm of $[Zn^{RR}L]^{2+}$ (20 μM) with **(*S*)-Ibuprofen**. λ_{ex} = 315 nm.

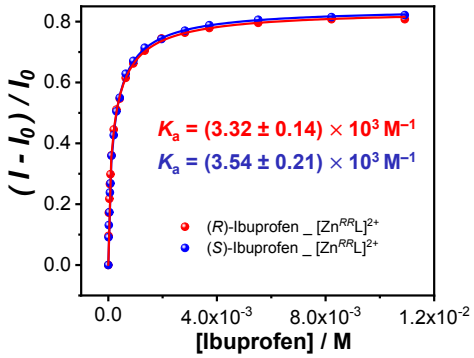

Figure S55. Overlaid binding isotherm of $[Zn^{RR}L]^{2+}$ (20 μM) with **(*R*)-Ibuprofen** (red) and **(*S*)-Ibuprofen** (blue). λ_{ex} = 315 nm.

$[Zn^{SS}L]^{2+}$ – Ibuprofen

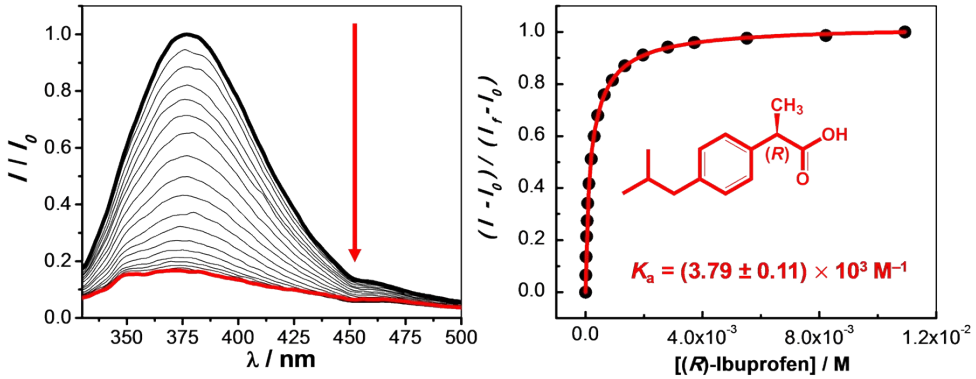

Figure S56. Titration profile and binding isotherm of **$[Zn^{SS}L]^{2+}$** (20 μM) with **(*R*)-Ibuprofen**. λ_{ex} = 315 nm.

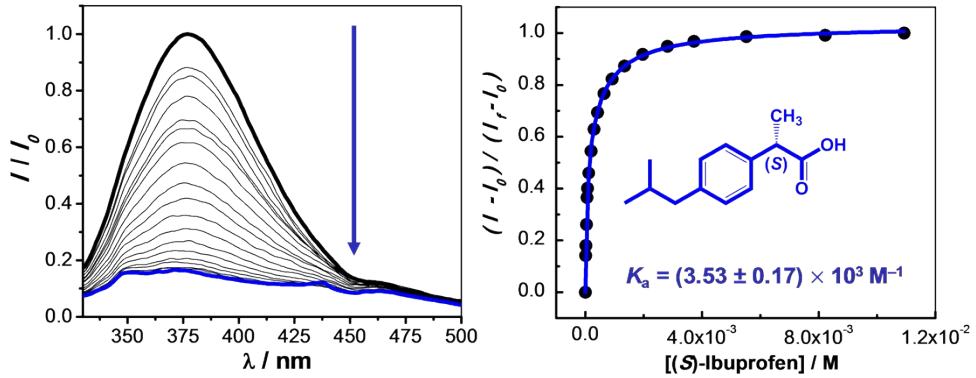

Figure S57. Titration profile and binding isotherm of **$[Zn^{SS}L]^{2+}$** (20 μM) with **(*S*)-Ibuprofen**. λ_{ex} = 315 nm.

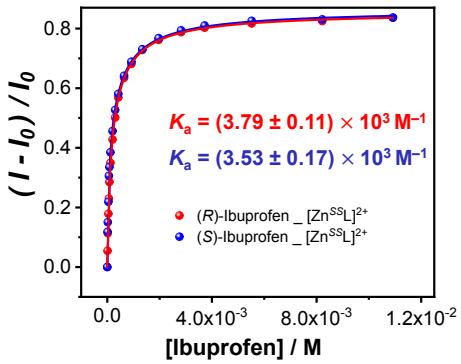

Figure S58. Overlaid binding isotherm of $[Zn^{SS}L]^{2+}$ (20 μM) with **(*R*)-Ibuprofen** (red) and **(*S*)-Ibuprofen** (blue). λ_{ex} = 315 nm.

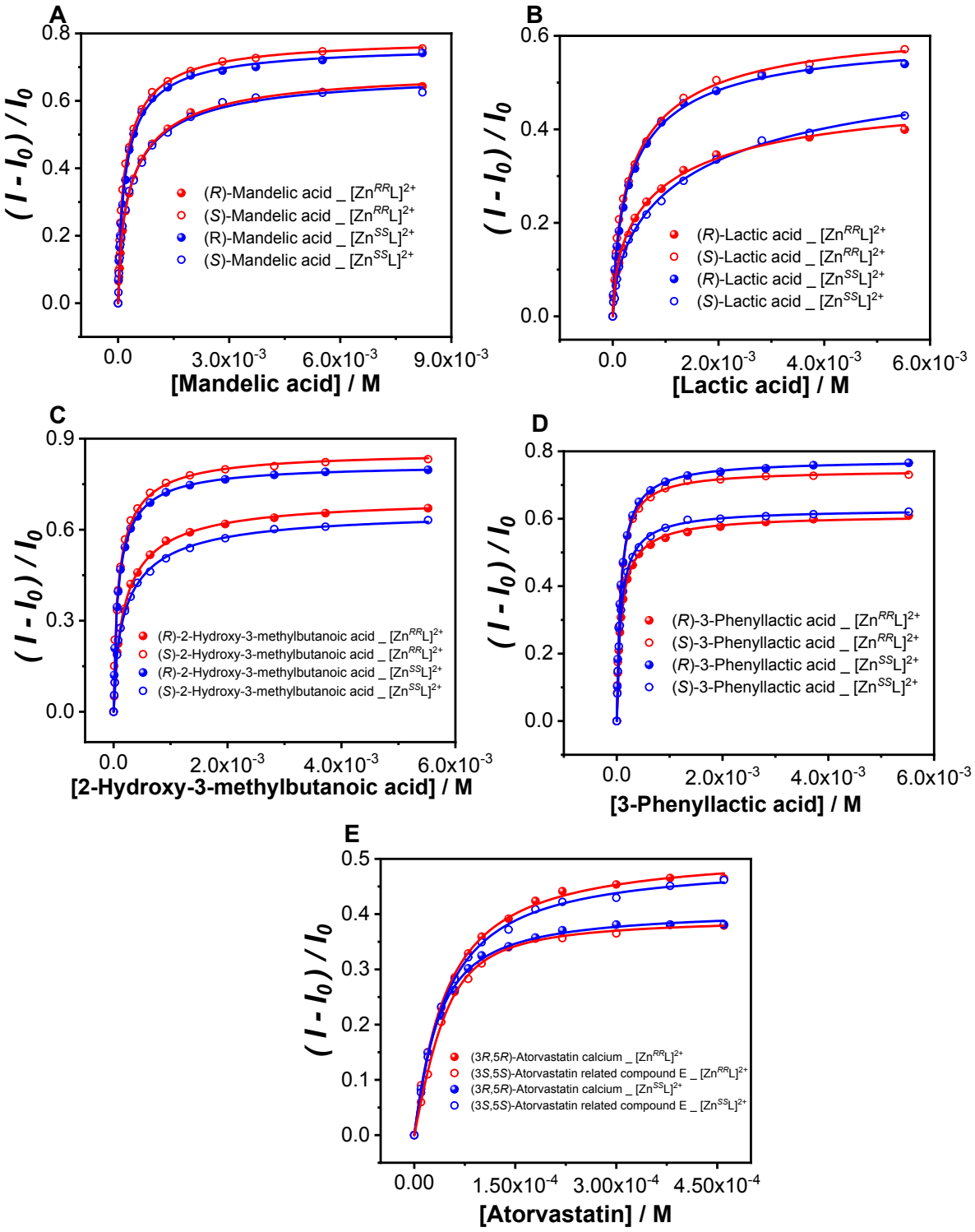

Figure S59. Overlaid binding isotherms showing the change in fluorescence intensity at the maximum wavelength of $[\mathbf{Zn}^{SS}\mathbf{L}]^{2+}$ and $[\mathbf{Zn}^{RR}\mathbf{L}]^{2+}$ (20 μM) obtained upon the addition of incremental amounts of either the (*R*)- or (*S*)-enantiomer of (A) mandelic acid, (B) lactic acid, (C) 2-hydroxy-3-methylbutanoic acid, (D) 3-phenyllactic acid, and (E) atorvastatin in MeCN/H_2O 7:3 at pH = 6 (MES, 50 mM). λ_{ex} = 315 nm.

$[Cu^{RR}L]^{2+}$ – Coumarin 343

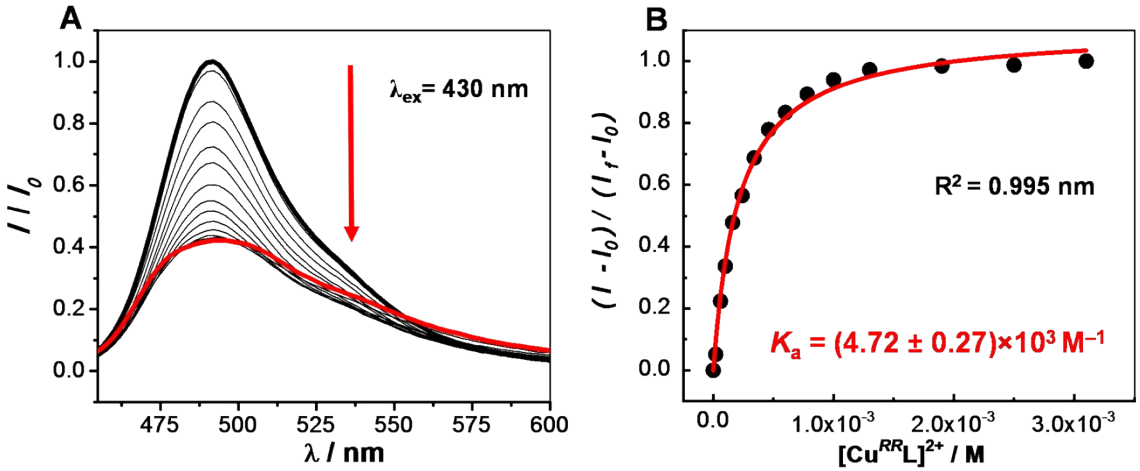

Figure S60. A) Fluorescence titration profiles of Coumarin 343 (0.01 μM) upon the addition of chiral receptor **$[Cu^{RR}L]^{2+}$** in MeCN/H_2O 7:3 at pH = 6 (MES = 50 mM); **B)** Titration isotherms based on the change in fluorescence intensity at the maximum wavelength of Coumarin 343 upon the addition of incremental amounts of **$[Cu^{RR}L]^{2+}$**. λ_{ex} = 430 nm. **$[Cu^{RR}L]^{2+}$** = 0 – 3 mM.

All solutions were prepared in MeCN/H_2O 7:3 at pH = 6 (MES = 50 mM). The concentrations used were: **$[Cu^{RR}L]^{2+}$** = 780 μM, [C343] = 0.01 μM.

[Cu^{RR}L•C343]$^{+}$ – Mandelic acid

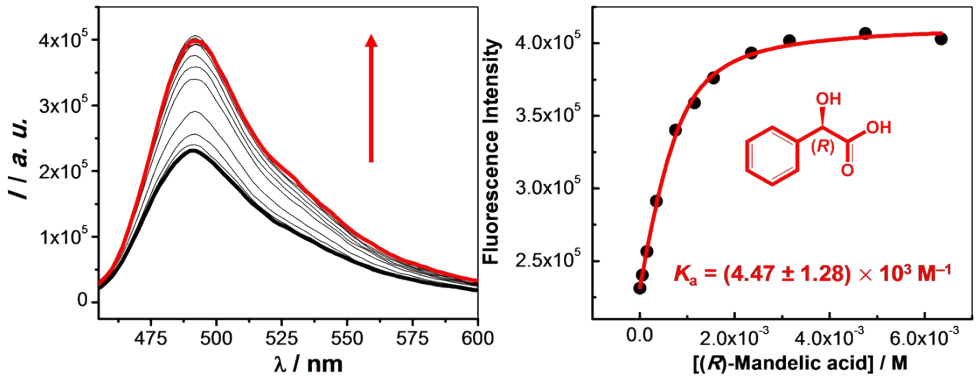

Figure S61. Titration profile and binding isotherm of **[Cu^{RR}L•C343]$^{+}$** (780 μM) with **(*R*)-mandelic acid**. λ_{ex} = 430 nm.

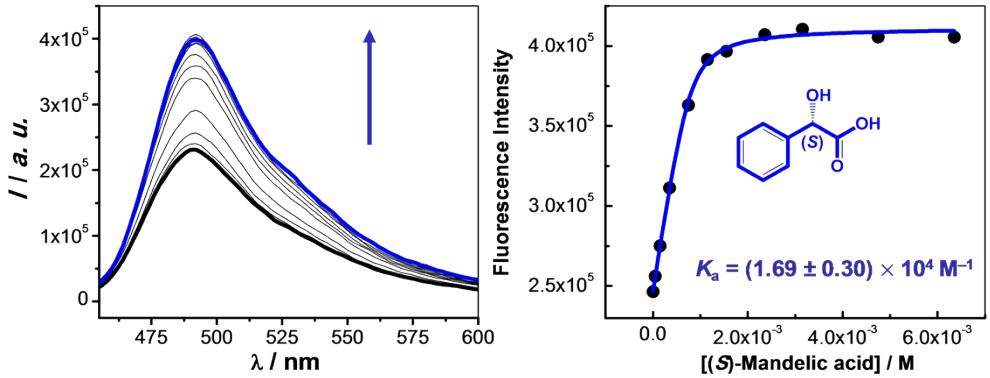

Figure S62. Titration profile and binding isotherm of **[Cu^{RR}L•C343]$^{+}$** (780 μM) with **(*S*)-mandelic acid**. λ_{ex} = 430 nm

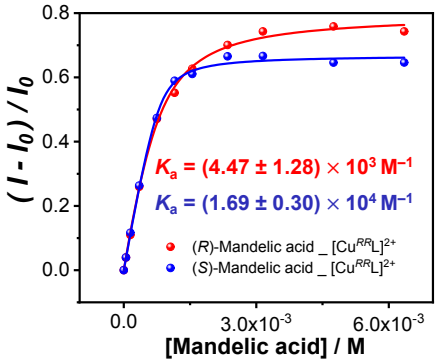

Figure S63. Overlaid binding isotherm of **[Cu^{RR}L•C343]$^{+}$** (780 μM) with **(*R*)-mandelic acid** (red) and **(*S*)-mandelic acid** (blue). λ_{ex} = 430 nm.

[Cu^{RR}L•C343]$^{+}$ – Lactic acid

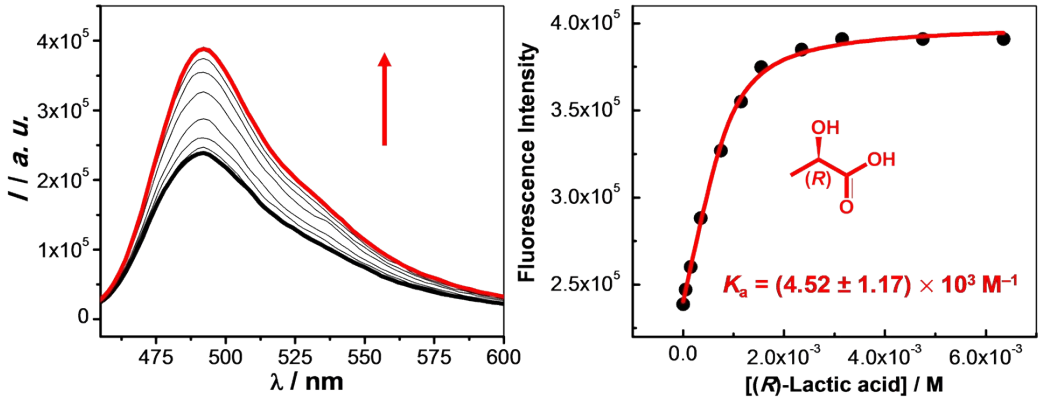

Figure S64. Titration profile and binding isotherm of **[Cu^{RR}L•C343]$^{+}$** (780 μM) with **(*R*)-Lactic acid**. λ_{ex} = 430 nm.

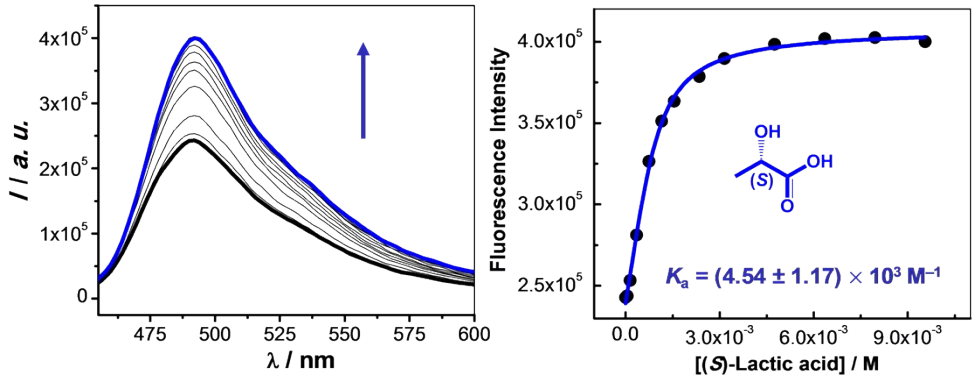

Figure S65. Titration profile and binding isotherm of **[Cu^{RR}L•C343]$^{+}$** (780 μM) with **(*S*)-Lactic acid**. λ_{ex} = 430 nm

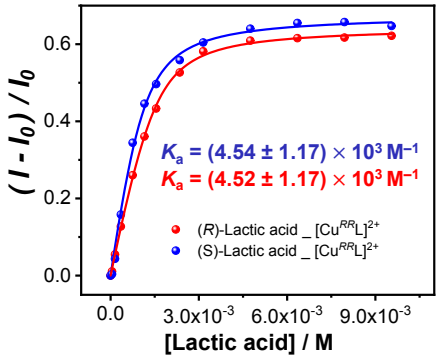

Figure S66. Overlaid binding isotherm of **[Cu^{RR}L•C343]$^{+}$** (780 μM) with **(*R*)-Lactic acid** (red) and **(*S*)-Lactic acid** (blue). λ_{ex} = 430 nm.

[Cu^{RR}L•C343]$^{+}$ – 2-Hydroxy-3-methylbutanoic acid

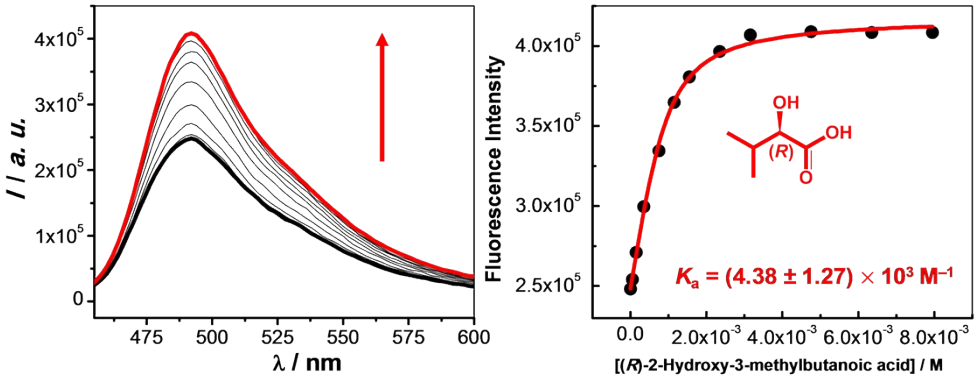

Figure S67. Titration profile and binding isotherm of **[Cu^{RR}L•C343]$^{+}$** (780 μM) with **(*R*)-2-hydroxy-3-methylbutanoic acid**. λ_{ex} = 430 nm.

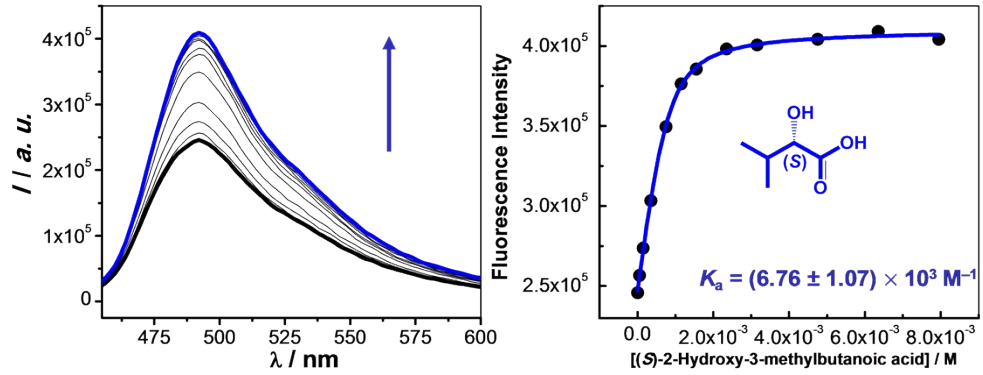

Figure S68. Titration profile and binding isotherm of **[Cu^{RR}L•C343]$^{+}$** (780 μM) with **(*S*)-2-hydroxy-3-methylbutanoic acid**. λ_{ex} = 430 nm.

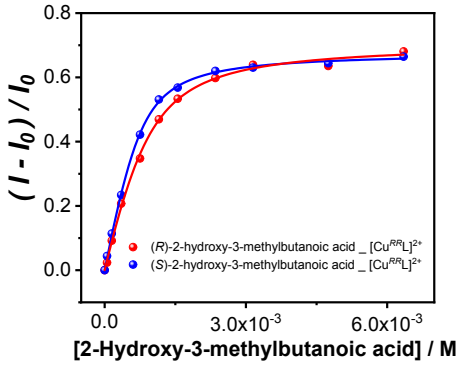

Figure S69. Overlaid binding isotherm of **[Cu^{RR}L•C343]$^{+}$** (780 μM) with **(*R*)-2-hydroxy-3-methylbutanoic acid** (red) and **(*S*)-2-hydroxy-3-methylbutanoic acid** (blue). λ_{ex} = 430 nm.

[Cu^{RR}L•C343]$^{+}$ – 3-Phenyllactic acid

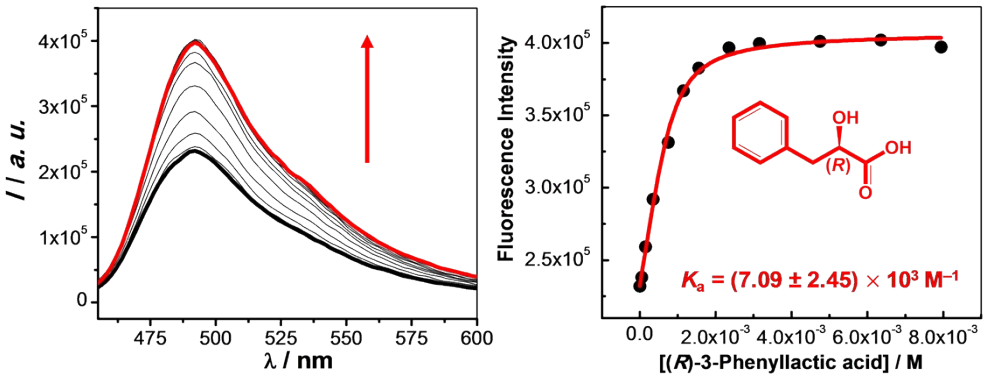

Figure S70. Titration profile and binding isotherm of **[Cu^{RR}L•C343]$^{+}$** (780 μM) with **(*R*)-3-phenyllactic acid**. λ_{ex} = 430 nm.

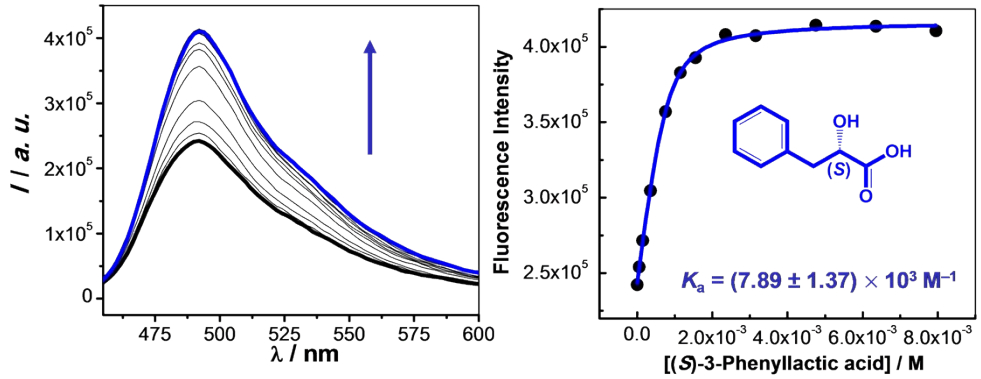

Figure S71. Titration profile and binding isotherm of **[Cu^{RR}L•C343]$^{+}$** (780 μM) with **(*S*)-3-phenyllactic acid**. λ_{ex} = 430 nm.

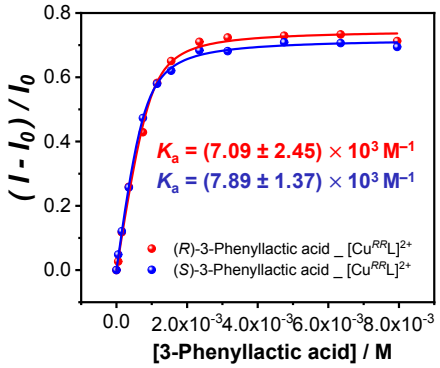

Figure S72. Overlaid binding isotherm of **[Cu^{RR}L•C343]$^{+}$** (780 μM) with **(*R*)-3-phenyllactic acid** (red) and **(*S*)-3-phenyllactic acid** (blue). λ_{ex} = 430 nm.

[Cu^{RR}L•C343]$^{+}$ – Phenylpropionic acid

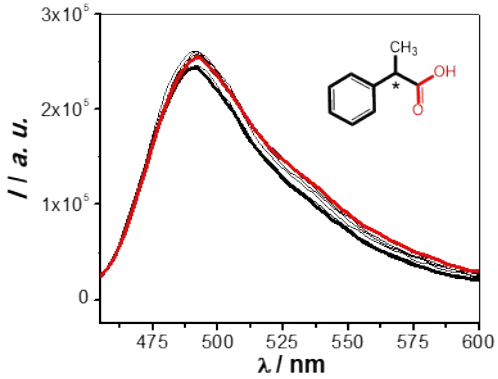

Figure S73. Titration profile of **[Cu^{RR}L•C343]$^{+}$** (780 μM) with (*S*)- or (*R*)-phenylpropionic acid. λ_{ex} = 430 nm.

7. Semi-Quantitative Analysis for the determination of enantiomeric excess (% *ee*)

The array experiments were performed using Aurora Microplates' 384-IQ-EB Evaporation Barrier, 384-wells microplates. The sensors and analytes solutions were dispensed using a Bionex Solutions Nanodrop Express 16-channel pipetting system, or a BNX 1536™ liquid handling system. Each experiment was performed in 24 repetitions. The sensor solutions and then the analyte solutions were dispensed in sequence; then, the microplates were centrifuged (2 min, 2500 rpm, T = 294 K) and read with a BMG CLARIOstar microplate reader.

For all experiments, the optic settings used for the simultaneous measurements of fluorescence intensity (FI) changes were as follow:

Channel	Exc. wavelength [nm]	Em. wavelength [nm]	Gain
1	300	380	1174
2	320	370	1967

The resulting emission data were subjected to the Student's T-test to exclude 4 data points out of 24 repetitions. The coefficient of variability within the class of same repetitions was lower than 4%. For semi-quantitative analyses, the data obtained were analyzed using linear discriminant analysis (LDA) without any further data pretreatment.

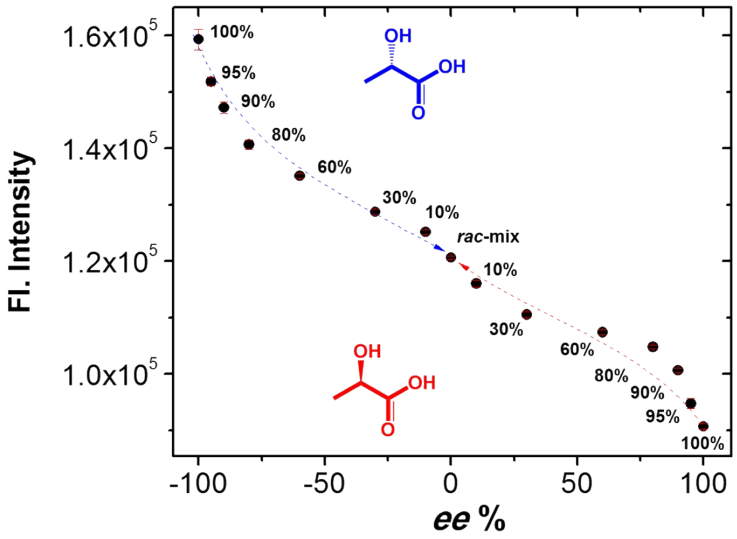

Figure S74. Results of simultaneous semi-quantitative analysis of enantiomeric excess determination (% *ee*) in (7/3 % v/v) at pH = 6 (MES, 50mM) for **lactic acid** using a sensor array based on **[Zn^{RR}L]$^{2+}$**. Array response represented in 2D plot for the range -100 to +100 % *ee* for both enantiomers. [Zn^{RR}L]$^{2+}$ = 20 μM, [lactic acid] = 2 mM.

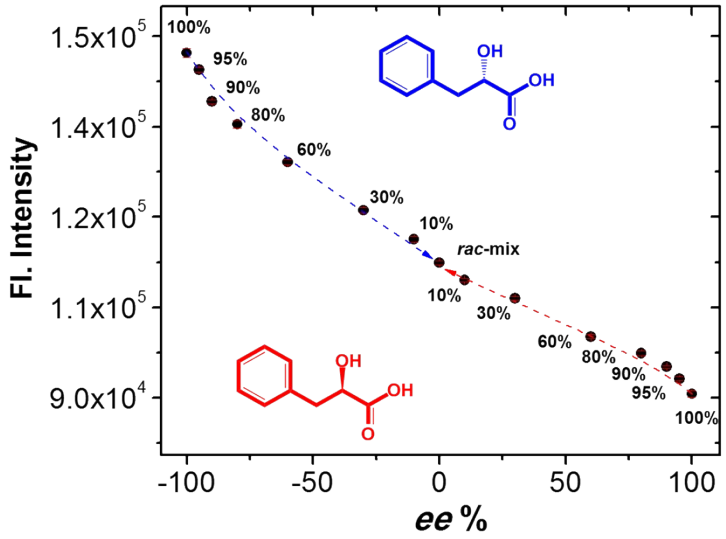

Figure S75. Results of simultaneous semi-quantitative analysis of enantiomeric excess determination (% *ee*) in (7/3 % v/v) at pH = 6 (MES, 50 mM) for **3-phenyllactic acid** using a sensor array based on **[Zn^{RR}L]$^{2+}$**. Array response represented in 2D plot for the range -100 to +100 % *ee* for both enantiomers. [Zn^{RR}L]$^{2+}$ = 20 μM, [3-phenyllactic acid] = 2 mM.

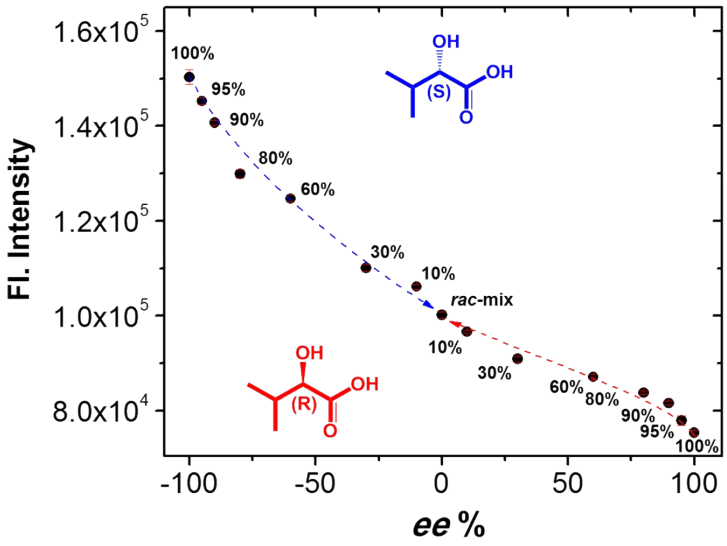

Figure S76. Results of simultaneous semi-quantitative analysis of enantiomeric excess determination (% *ee*) in (7/3 % v/v) at pH = 6 (MES, 50 mM) for **2-hydroxy-3-methylbutanoic acid** using a sensor array based on **[Zn^{RR}L]$^{2+}$**. Array response represented in 2D plot for the range -100 to +100 % *ee* for both enantiomers. [Zn^{RR}L]$^{2+}$ = 20 μM, [2-hydroxy-3-methylbutanoic acid] = 2 mM.

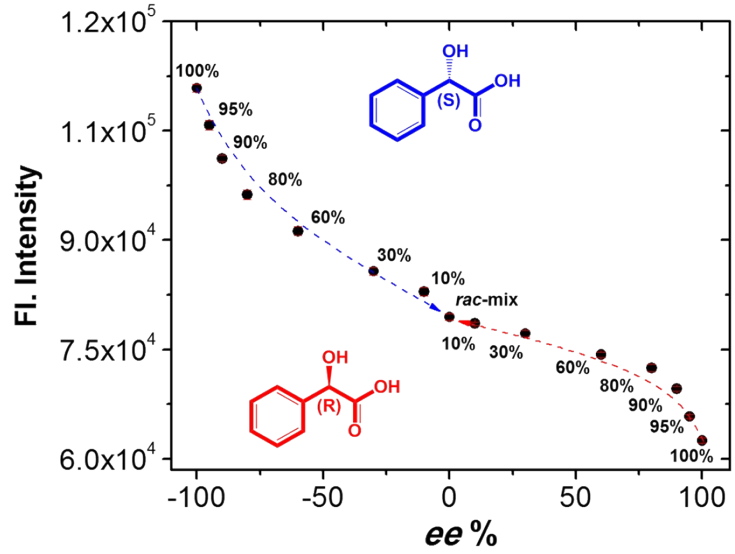

Figure S77. Results of simultaneous semi-quantitative analysis of enantiomeric excess determination (% *ee*) in (7/3 % v/v) at pH = 6 (MES, 50 mM) for **mandelic acid** using a sensor array based on **[Zn^{RR}L]$^{2+}$**. Array response represented in 2D plot for the range -100 to +100 % *ee* for both enantiomers. [Zn^{RR}L]$^{2+}$ = 20 μM, [mandelic acid] = 2 mM.

8. Quantitative linear regression analysis of enantiomeric excess (% *ee*)

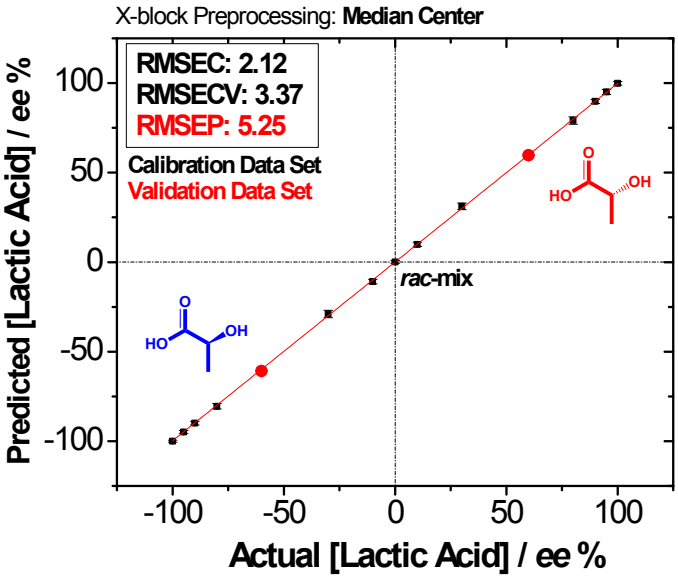

Figure S78. The results of simultaneous quantitative linear regression analysis of enantiomeric excess using support vector machine (SVM) algorithm for lactic acid.

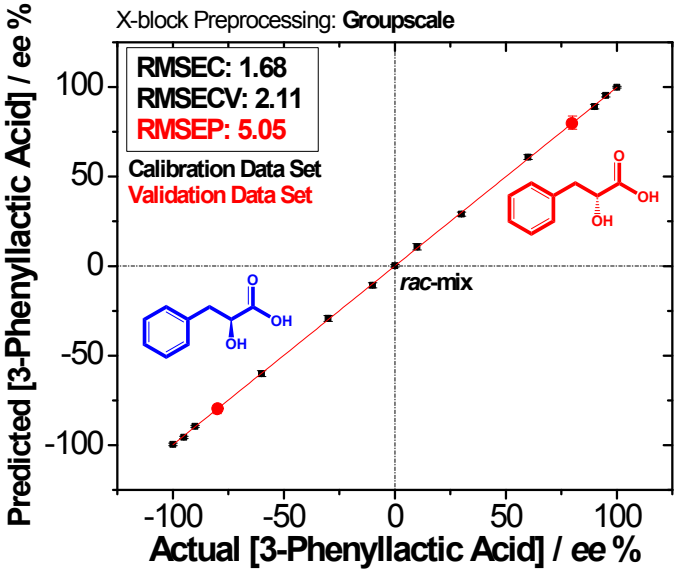

Figure S79. The results of simultaneous quantitative linear regression analysis of enantiomeric excess using support vector machine (SVM) algorithm for 3-phenyllactic acid.

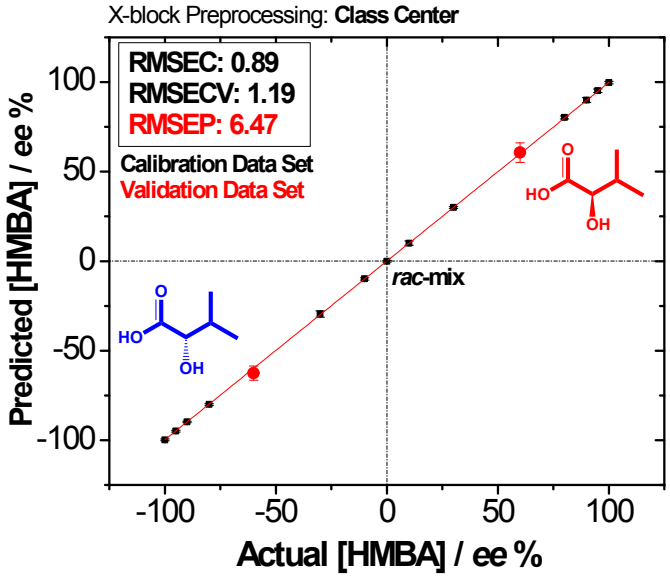

Figure S80. The results of simultaneous quantitative linear regression analysis of enantiomeric excess using support vector machine (SVM) algorithm for 2-hydroxy-3-methylbutanoic acid.

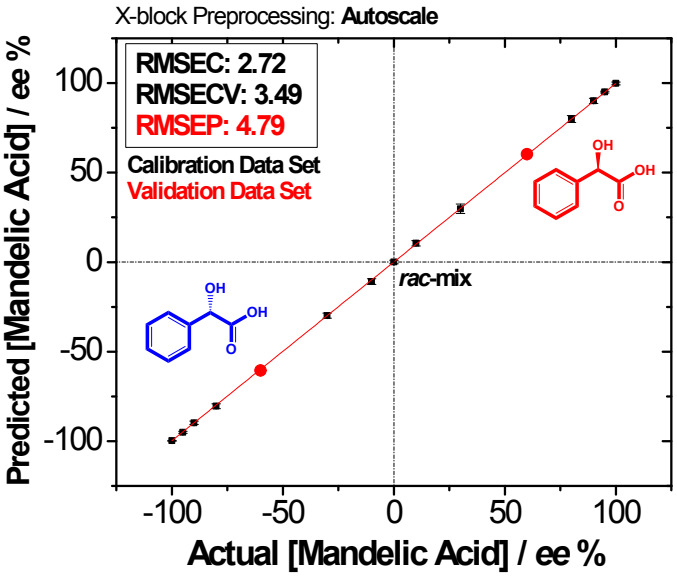

Figure S81. The results of simultaneous quantitative linear regression analysis of enantiomeric excess using support vector machine (SVM) algorithm for mandelic acid.

9. Stoichiometry determination: Job's plot

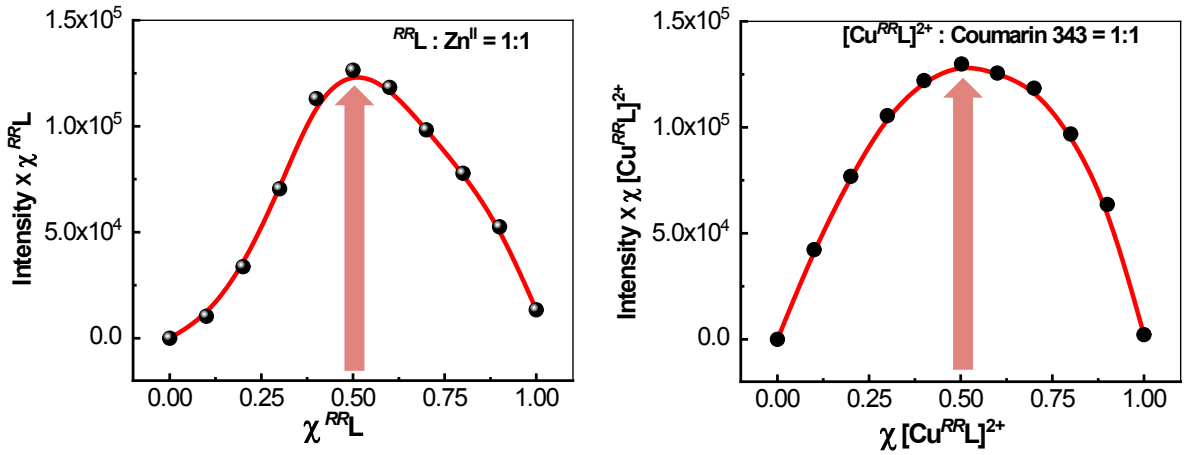

Figure S82 Job's plot for the determination of the stoichiometry of (A) $Zn(NO_3)_2$ and chiral ligand ^{RR}**L**; (B) **[Cu^{RR}L]$^{2+}$** and Coumarin 343 in CH_3CN:H_2O 7:3 at pH = 6 (MES, 50 mM).

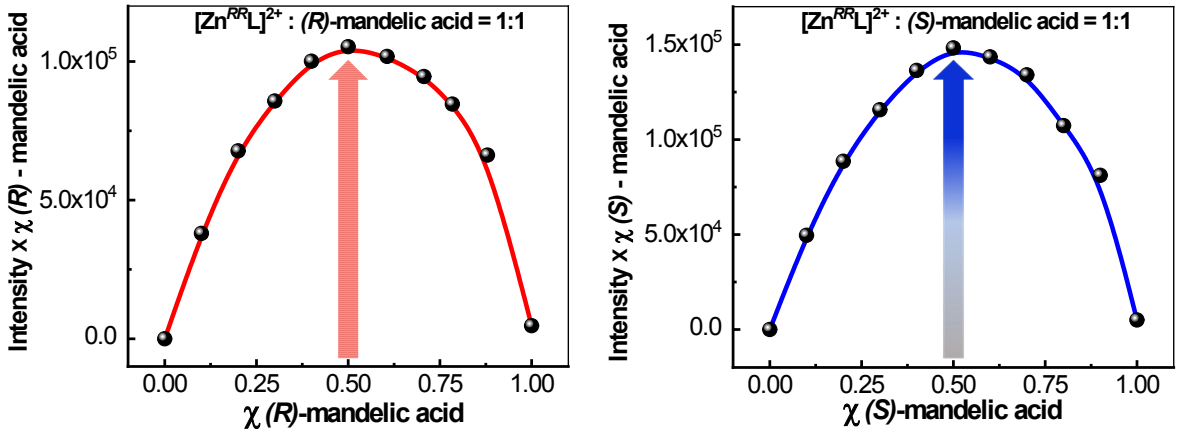

Figure S83. Job's plot for the determination of the stoichiometry of (A) **[Zn^{RR}L]$^{2+}$** and *(R)*-mandelic acid; (B) **[Zn^{RR}L]$^{2+}$** and (*S*)-mandelic acid in CH_3CN:H_2O 7:3 at pH = 6 (MES, 50 mM).

10. References

(1) Ravikumar, I.; Ghosh, P. *Inorg. Chem.* **2011**, *50*, 4229–4231.

(2) Connors, A. K. Binding Constants: the Measurement of Molecular Complex Stability; Wiley: New York, 1987.

(3) Schalley, C. A. *Analytical Methods in Supramolecular Chemistry*; John Wiley & Sons, 2012.

(4) Hill, Z. D.; MacCarthy, P. *J. Chem. Educ.* **1986**, *63*, 162–167.

(5) MacCarthy, P. *Anal. Chem.* **1978**, *50*, 2165–2165.